Universidade de Aveiro
Departamento de Electrónica, Telecomunicações e Informática,
2019

Cláudia Gonçalves Rodrigues

Development of an ONT for NG-PON2

Desenvolvimento de uma ONT para sistemas NG-PON2

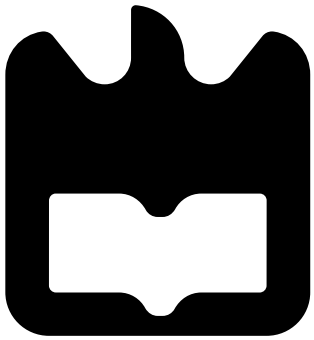

Cláudia Gonçalves Rodrigues

Desenvolvimento de uma ONT para sistemas NG-PON2

Dissertação apresentada à Universidade de Aveiro para cumprimento dos requesitos necessários à obtenção do grau de Mestre em Engenharia Eletrónica e Telecomunicações, realizada sob a orientação científica de Dr. António Teixeira e Dr. Mário Lima, Professores do Departamento de Eletrónica da Universidade de Aveiro e do Engenheiro Francisco Rodrigues, da PICadvanced, S.A.

Dedico este trabalho aos meus pais, e irmã

o júri / the jury

presidente / president	**Professor Doutor João Nuno Pimentel da Silva Matos** Professor Associado da Universidade de Aveiro (por delegação da Reitoria da Universidade de Aveiro)
vogais / examiners committee	**Professor Doutor António Luís Jesus Teixeira** Professor Associado C/ Agregação da Universidade de Aveiro (orientador)
	Professora Doutora Maria do Carmo Raposo de Medeiros Professor Associado da Universidade de Coimbra

agradecimentos / acknowledgements

Nesta etapa que marca o concluir da minha formação, gostaria de começar por agradecer aos meus orientadores, Prof. António Teixeira e Engenheiro Francisco, assim como ao Prof. Mário Lima pelo conhecimento transmitido, pela disponibilidade e pelo auxílio prestado sempre que necessário. À Carla, sendo uma ponte entre a família e o meio académico, que foi um modelo a seguir neste processo, uma ajuda indispensável com as palavras certas e o maior apoio nesta última fase académica. Não podia deixar de referir também a minha madrinha, a tia Lurdes, que marcou a palavra que não me deixou desistir a meio deste percurso e se mostrou sempre um apoio constante na minha vida. Ao André e ao Ruben, que marcaram estes últimos anos da melhor maneira e que também muito facilitaram este percurso com os seus apontamentos. Ao João que me fez companhia em vários momentos de estudo mas também de diversão. Ao Carlos, que foi o apoio mais presente e fundamental em todas as etapas, cuja ajuda eu não posso nunca retribuir na mesma quantidade, cujo carinho e atenção foram essenciais para a motivação não desaparecer. Obrigada. Por último, aos responsáveis do que eu sou hoje e do que irei ser daqui para a frente, à minha irmã, ao meu cunhado e aos meus pais, que nunca deixaram de acreditar em mim e sempre me deram força nos momentos mais difíceis. Esta meta é tão vossa quanto minha. Nunca vou conseguir agradecer-vos o suficiente.

palavras chave Comunicações óticas, Next Generation Passive Optical Network 2 (NG-PON2), Optical Network Termination (ONT), multiplexagem de canais, Circuitos Óticos Integrados

Resumo A constante eclosão de novos produtos e serviços através das redes de comunicação, nomeadamente a internet, ocasiona a procura por tecnologia capaz de fornecer estes serviços respondendo com cada vez maiores velocidades e largura de banda. Actualmente, a tecnologia apta para estas características é a comunicação via fibra ótica (comunicações óticas). Esta tecnologia é aplicada sob redes Passive Optical Network (PON), arquitecturas que realizam a distribuição de fibra desde a origem (Optical Line Terminal (OLT)) até ao consumidor final (ONT ou Optical Network Unit (ONU)). É no contexto destas redes que surge a aplicaçao de ótica integrada para implementação destas estruturas (OLTs e ONTs) para transmissão e envio de informação com redução de consumo de energia, de complexidade e, por fim, de tamanho. Assim sendo, estes chips pretendem incluir num único exemplar, vários componentes óticos replicando as suas funções em tamanhos muito reduzidos, com recurso a elementos maioritariamente passivos. Esta dissertação contribui assim com o desenvolvimento de novas soluções para implementação de futuras redes capazes de dar resposta aos requisitos dos utilizadores. Deste modo, pretende-se desenvolver uma arquitectura para a implementação de um transmissor em formato Photonic Integrated Circuit (PIC), a ser implementado no lado do cliente - ONT. Este PIC deverá conseguir atingir uma taxa de transmissão de 40 Gbit/s e, para tal, deverá ainda ser estudado um método de implementação da técnica de multiplexagem de canais que adicione poucas perdas ao sistema, mas que, ainda assim, permita obter os 40 Gbit/s à saída pretendidos. A arquitectura proposta deverá ainda garantir um mínimo de 8 dBm de potência ótica à saída. Além disto, o chip deve ser concordante com os requisitos de rede impostos pela norma NG-PON2. Este trabalho é financiado pelo Fundo Europeu de Desenvolvimento Regional (FEDER), através do Programa Operacional Regional do Centro (CENTRO 2020) do Portugal 2020 [Projeto HeatIT com o n° 017942 (CENTRO-01-0247-FEDER-017942)]

keywords Optical communications, NG-PON2, ONT, channel multiplexing, PIC

Abstract

The constant emergence of new products and services through communication networks, namely the Internet, leads to the demand for technology capable of providing these services with increasing speeds and bandwidth. Nowadays, the technology suitable to provide these features is communication through an optical fiber (optical communications). This technology is applied by PON networks, in which architectures distribute optical fiber from the central office (OLT) through the final user (ONT or ONU). It is in the context of these networks that arise the integrated optical applications for implementation of these structures (OLTs and ONTs) for data transmission and reception with reduced energy consumption, complexity as well as size. Therefore, these chips pretend to include, in one single copy, several optical components multiplying its functionalities in very reduced sizes and, for power consume reduction, using mostly passive elements. This dissertation intends to contribute with new solutions development for implementation of new structures capable to meet the user needs, with a development of a new architecture for implementing a PIC transmitter to be integrated on the client-side at the ONT. The optoelectronic solution should be capable of address 40 GBit/s of data rate and, for that, it should also be evaluated an implementation method to apply channel multiplexing to the system that, at the same time that it allows the 40 Gbit/s bit rate output, presents low additional loss values to the system. The proposal architecture should also ensure an 8 dBm of minimum output optical power. Besides, the final chip must be compliant with NG-PON2 network requirements.

Contents

List of Figures

List of Tables

Acronyms

BER	Bit Error Ratio
B2B	Back-to-Back
BB	Building Block
CW	Continuous Wave
DFB	Distributed Feedback Laser
DML	Direct Modulated Laser
DS	Downstream
EAM	Electro-Absorption Modulator
EME	bidirectional Eigenmode Expansion
EML	External Modulated Laser
ER	Extinction Ratio
FP-SOA	Fabry-Perot Semiconductor Power Amplifier
FTTH	Fiber To The Home
GI-MMF	Graded Index Multimode Fiber
G-PON	Gigabit-capable Passive Optical Network
GSG	Ground-Signal-Ground
FhG-HHI	Fraunhofer Heinrich Hertz Institute
InP	Indium Phosphide
ISI	Intersymbol Interference
ITU	International Telecommunication Union
LED	Light Emitting Diode
MMF	Multi Mode Fiber
MMI	Multimode Interferometer
MPA	guided-Mode Propagation Analysis
MPW	Multi Project Wafer
NG-PON2	Next Generation Passive Optical Network 2
NRZ	Non-Return to Zero
ODN	Optical Distribution Network
OEO	Optical-Electrical-Optical
OLT	Optical Line Terminal
ONT	Optical Network Termination
ONU	Optical Network Unit
OOK	On-Off Keying
PDK	Process Design Kit
PE	Error Probability
PIC	Photonic Integrated Circuit
PIN	p-i-n photodiode
PON	Passive Optical Network
PtP	Point-to-Point
RE	Reach Extender
RI	Refractive Index
ROP	Received Optical Power
SI-MMF	Step Index Multimode Fiber
SMF	Single Mode Fiber
SOA	Semiconductor Optical Amplifier
SSC	Spot-Size Converter
TE	Transverse Electric
TM	Transverse Magnetic
TWDM	Time and Wavelength Division Multiplexing
TW-SOA	Travelling-Wave Semiconductor Power Amplifier
US	Upstream
XG-PON	10-Gigabit Passive Optical Network
WDM	Wavelength Division Multiplexing
WM	Wavelength Multiplexer

Chapter 1

Introduction

This chapter briefly introduces the topic and scope of this thesis. Firstly, an overview and motivation (section 1.1) are presented, then the main goals of the dissertation and finally, in sections 1.3 and 1.4, it is described the structure of the document and its contributions.

1.1 Overview and Motivation

For the past 20 years, society's relationship with the Internet and its services has suffered an exponential growth, mainly due to people's dependence on the internet and its services. Nowadays, besides being useful, Internet has become essential in the business world, sector of activity that has experienced the greatest turnaround of all, reaching the point where new work positions have emerged from it.

Therefore, it is constantly required the improvement of the Internet in order to facilitate its access, but also to get faster and cheaper for all sectors, mainly focusing on those depending on Internet to be profitable. Once telecommunication networks, where this tool is inserted, are a very explored area, the technologies commonly used became very saturated and inefficient for the growing demand. This is where optical communications research takes place since this is the fastest and with greater capacity communication technology currently known [7].

Figure 1.1 shows the broadband access data rates evolution for the past 35 years.

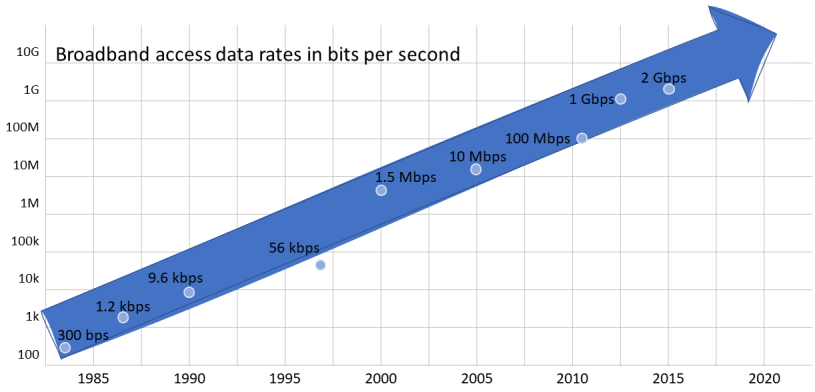

Figure 1.1: Growing access capacity along the last years. (Based in [1])

In the last few years, an evolution has been clear in implementation and development of

provision of fiber to the final user (technically referred as Fiber To The Home (FTTH)).

Over the last few years, PON networks were developed and standardized by entities as ITU or IEEE. These organizations were concern about the growing demand for higher bandwidth and the number of new users [8]. Starting with the Gigabit-capable Passive Optical Network (G-PON), from the 10-Gigabit Passive Optical Network (XG-PON) until the emergence of NG-PON2, the capacity and distance reach was always improved [9] .

The technology evolution of the physical layer leads also to a processing deployment in ONT and OLT. Consecutively, this leads to the development of hardware and software specific for OLT in order to respond to their requirements but still delivering a good performance.

With that being said, this dissertation presents an architecture for an ONT with channel multiplexing for NG-PON2 systems.

1.2 Objectives

The aim of this work is to project an architecture of an integrated photonic transceiver for NG-PON2 networks. To conclude this, the detailed objectives are:

- Study the NG-PON2 requirements and specifications;
- Simulate direct and external modulation scenarios and analyse which one is the most suitable for NG-PON2;
- Propose a transmitter architecture for NG-PON2 standard;
- Implement the mask layout of the proposed PIC.

1.3 Structure

This work is divided into 6 chapters:

1. Introduction
2. Access network description
3. Photonic Integrated Circuits and its components
4. Multimode Interferometer
5. ONT transmitter architecture for NG-PON2 systems
6. Conclusions and Future Work

The first chapter presents the context and motivation of this dissertation, as well as its objectives, structure and contributions.

In chapter two are described and detailed several requirements for the implementation of a NG-PON2 network.

Right after, the third chapter has a description of PICs technology next to the description of several PIC components, followed by its simulation using the INTERCONNECT software from Lumerical.

The fourth chapter describes the multimode interferometers state of the art and then a step by step implementation of a 1x4 MMI.

In the fifth chapter is presented the proposal architecture for ONT.

At last, the document closes with a chapter with final conclusions and future work.

1.4 Contributions

The main contributions of this work are:

- A 1x4 MMI coupler with SmartPhotonics stack of materials for capable of working on the specific range from 1535.68 nm to 1535.04 nm from NG-PON2 standard (first four channels of C band);
- A 1x4 MMI coupler with SmartPhotonics stack of materials for capable of working on the specific range from 1596.34 nm to 1598.89 nm from NG-PON2 standard (first four channels of L band);
- Design of a PIC architecture for an ONT transmitter implementation for NG-PON2 systems;

Chapter 2

Access networks

The increasing demand for higher bandwidth impose telecommunications operators to seek for technologies to answer these demands. In response, optical communications received special attention due to its several advantages and response to bandwidth request. In this chapter a brief introduction to PON networks is made, followed by a full description of the NG-PON2 systems requirements and standard definitions.

2.1 Passive Optical Networks

PONs are based on a point-to multi-point architecture that enables the service providers to serve the end user. The key elements in these networks are the OLTs, the ODN and the ONT/ONU [10].

Usually the OLT is located in a central office, the ONT/ONU is in the end-user's buildings and the ODN, as the name indicates, is the structure involving all the fibers and splitters outside the ONT and OLT [11]. Figure 2.1 addresses a PON networks with the multiple key elements that composes it.

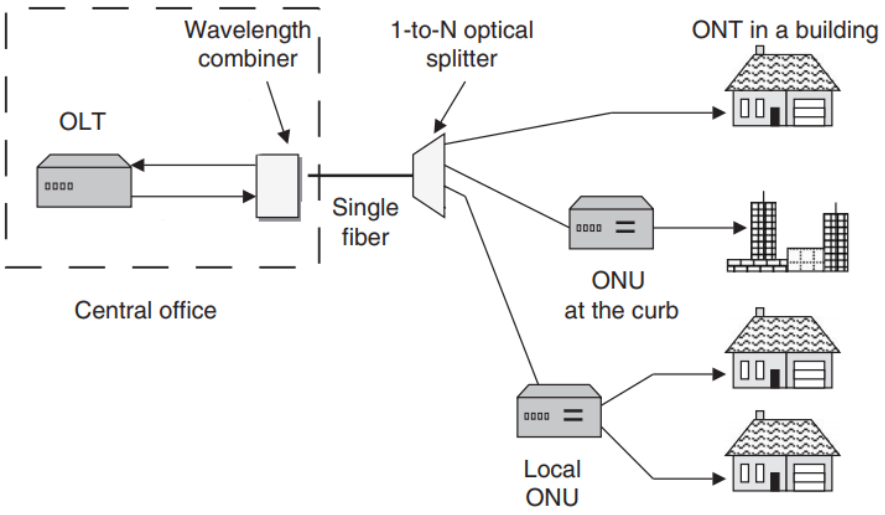

Figure 2.1: Fundamental building blocks of a PON. (Based on [2])

As the name suggest, in PONs all the elements included should be passive, which means that there is no needed for power supply in order to operate the ODN.

2.2 Next Generation Passive Optical Networks 2

As it was already described, along the years there has been a consecutive improvement in the PON technologies. The NG-PON2 is one of the latest access network technology to be standardize being its last renovation in this present year, 2019, by ITU-T (Telecommunication standardization sector of ITU) [12]. In Figure 2.2 it is possible to see the PON's technology evolution through the years (considering only the ITU standards).

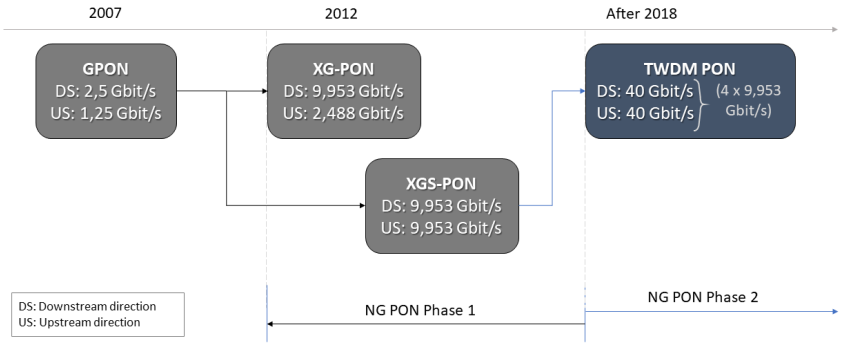

Figure 2.2: PON standards evolution from ITU (Based on [3])

NG-PON2 addresses multiple parameters and requirements in order to guide and motivate the convergence between the physical layer and the transmission layer specifications, being, at the same time, completely compatible with previous implementations such as G-PON, XG-PON and so on, as it is possible to observe in Figure 2.3.

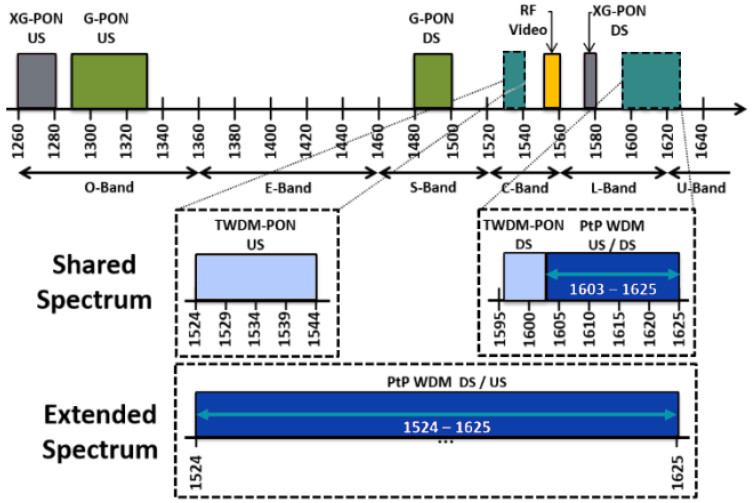

Figure 2.3: Optical spectrum coexistence for multiple access technologies. [4]

However, coexistence of these access networks, may require mitigation techniques in order

to avoid some inter-system impairments [12].

In Figure 2.4 it is possible to observe the reference architecture for the multi-wavelength NG-PON2 system.

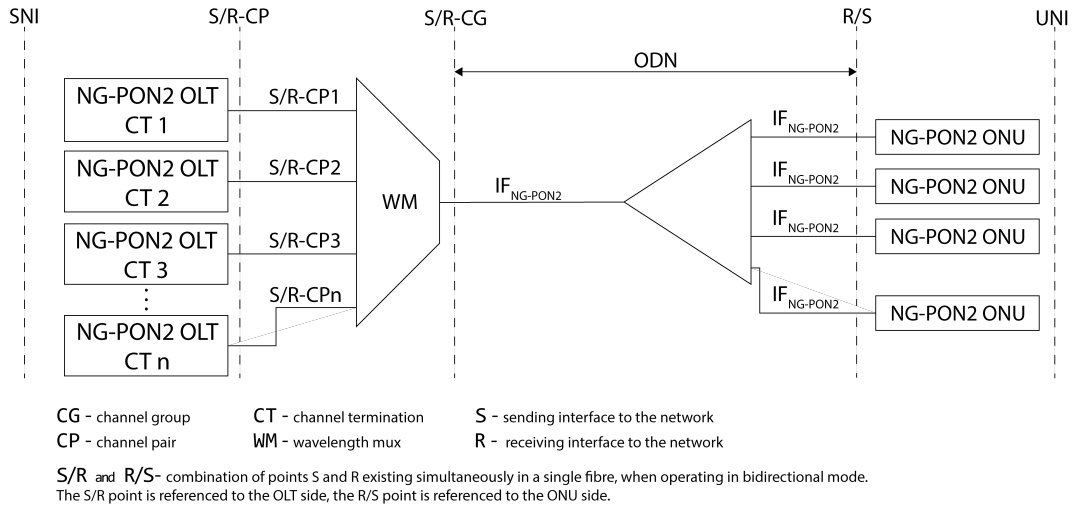

Figure 2.4: NG-PON2 reference logical architecture. (Based on [11])

Each ONU is composed by a transmitter and a receiver for correspondent US and DS bands. The Wavelength Multiplexer (WM) connected to multiple OLT units allows channel multiplexing [12].

The two directions for data transmission in the ODN are identified as follows:

- DS direction for signals travelling from the OLT to the ONU(s);
- US direction for signals travelling from the ONU(s) to the OLT [12].

Both directions travel through the same fiber and components [12]. This access network offers Time and Wavelength Division Multiplexing (TWDM) as the transmission technique and an optional Point-to-Point (PtP) system that can be used in an overlay to TWDM with the capability of bidirectional data transmission between OLT and ONU [12].

2.2.1 Requirements

In this section it will be used the recommendation G.989 [12] by ITU-T to detail the NG-PON2 requirements for implementation.

2.2.1.1 Bit rate

NG-PON2 systems must have a minimum of four channel pairs (US and DS directions) in a TWDM architecture, and a maximum of eight. The bit rate available for the system varies accordingly with the number of channel pairs it is being used. For the minimum of four channel pairs, there are three combinations of bit rates per wavelength:

- 2.5 Gbit/s for US and 10 Gbit/s DS;

- 2.5 Gbit/s for US and DS;
- 10 Gbit/s for US and DS [12].

So, in this case, the transmission capacities vary between 10 Gbit/s and an aggregate capacity of 40 Gbit/s when channel multiplexing is applied and, when adding more channels, the maximum value of 8 channel pairs, the transmission capacity can rise up to 80 Gbit/s [12].

2.2.1.2 Fiber reach

The maximum fibre distance, between S/R-CG and R/S point in Figure 2.4, without Reach Extender (RE), is 20km for DD20, and 40 km for DD40, but using RE, it is possible to reach 60 km. These specifications are considered for fiber type of [ITU-T G.652][13] or compatible [12].

2.2.1.3 Wavelength plan

The wavelength bands for NG-PON2 are listed in Table 2.1.

TWDM PON		**PtP WDM PON**
DS (nm)	US (nm)	DS/US (nm)
1596-1603	Wide Band: 1524-1544 Reduced Band: 1528-1540 Narrow Band: 1532-1540	Expanded Spectrum: 1524-1625 Shared Spectrum: 1603-1625

Table 2.1: NG-PON2 wavelength bands. [11]

The wavelength plan of NG-PON2 is designed to allow the coexistence in the spectrum with the already implemented PON systems, RF video overlay and TWDM [12]. As it is possible to see in Table 2.1, in PtP Wavelength Division Multiplexing (WDM) PON, the shared spectrum allows the coexistence of the mentioned systems, even if, for more bandwidth, in absence of any of these coexistence systems, the expanded spectrum can be used.

On the other hand, also in Table 2.1, TWDM PONs, for US direction, provides 3 wavelength bands: wide band, reduced band and narrow band. The narrow band is the smaller in terms of bandwidth, and, for that reason, it also presents the smallest channel spacing from the three. The implementation of systems using this band will require a light source with a narrow linewidth, limiting the laser options to use due to the reduced available spectrum in this band. Despite that, this limiting factor can be compensated by the possibility of shortening the laser tuning range due to the fact that the channels are closer.

Considering the narrow band, the central frequency and the corresponding wavelength of the maximum available channels for DS and US directions, stated by NG-PON2 in [12] are presented in Table 2.2.

	Downstream (L Band)		*Upstream (C Band)*	
Channel	***Central Frequency (THz)***	***Wavelength (nm)***	***Central Frequency (THz)***	***Wavelength (nm)***
1	187.8	1596.34	195.6	1532.68
2	187.7	1597.19	195.5	1533.47
3	187.6	1598.04	195.4	1534.25
4	187.5	1598.89	195.3	1535.04
5	187.4	1599.75	195.2	1535.82
6	187.3	1600.60	195.1	1536.61
7	187.2	1601.46	195.0	1537.40
8	187.1	1602.31	194.9	1538.19

Table 2.2: NG-PON2 US and DS channels (Narrow band). [11]

2.2.1.4 ODN Optical Path Loss Classes

There are four ODN classes: N1, N2, E1 and E2. The optical path loss for each one of these classes is specified between the S/R-CG and R/S reference points from Figure 2.4 [12].

	Class			
Parameter	***N1 (dB)***	***N2 (dB)***	***E1 (dB)***	***E2 (dB)***
Minimum optical path loss	14	16	18	20
Maximum optical path loss	29	31	33	35
Maximum differential optical path loss	15 dB			

Table 2.3: ODN optical path loss classes. [11]

The minimum loss values referred in Table 2.3 can be exceeded by ODN's gain elements (as amplifiers or repeaters), wavelength couplers and low split ratio power splitters, but, for that, the ODN must contain attenuators in order to guarantee the maximum optical path loss for the given class, preventing BER degradation and/or potential damage to receivers [12].

2.2.1.5 ONU/ONT Requirements

As seen before in 2.2.1.1, there are several bit rates available, concerning the number of channel pairs chosen [12]. Also, in NG-PON2 it is possible to have tunable ONUs which are structures equipped with a tunable transmitter and receiver, making possible to the ONU to tune between the channels and also to select the channel to be recovered. Based on tunability, ONUs can be mainly divided into 3 classes:

- Class 1: tuning time bellow 10 μs;
- Class 2: tuning time between 10 μs and 25 ms;
- Class 3: tuning time between 25 ms and 1 s [12].

The requirements for the ONU will then vary according to these two factors: the bit rate and the link type, but also with the ODN class. The Tables 2.4 and 2.5 describes this requirements for, respectively, 2.5 Gbit/s and 10 Gbit/s.

Block	Parameter	Value			
Transmitter	*Nominal line rate*	2.48832 Gbit/s			
	Minimum operating channel spacing	50 GHz			
	Maximum operating channel spacing	200 GHz			
	Line code	Scrambled Non-Return to Zero (NRZ)			
	ODN class	N1	N2	E1	E2
	Mean channel launch power minimum				
	Type A link	+4 dBm	+4 dBm	+4 dBm	+4 dBm
	Type B link	0 dBm	0 dBm	0 dBm	0 dBm
	Mean channel launch power maximum				
	Type A link	+9 dBm	+9 dBm	+9 dBm	+9 dBm
	Type B link	+5 dBm	+5 dBm	+5 dBm	+5 dBm
	Minimum Extinction Ratio (ER)	8.2 dBm			
Receiver	*BER reference level*	10^{-4}			
	ODN class	N1	N2	E1	E2
	Sensitivity	-30 dBm	-30 dBm	-30 dBm	-30 dBm
	Overload	-10 dBm	-10 dBm	-10 dBm	-10 dBm

Table 2.4: Optical Interface parameters of the ONU for 2.5 Gbit/s. [11]

Block	Parameter	Value			
Transmitter	*Nominal line rate*	9.95328 Gbit/s			
	Minimum operating channel spacing	50 GHz			
	Maximum operating channel spacing	200 GHz			
	Line code	Scrambled NRZ			
	ODN class	N1	N2	E1	E2
	Mean channel launch power minimum				
	Type A link	+4 dBm	+4 dBm	+4 dBm	NA
	Type B link	+2 dBm	+2 dBm	+2 dBm	+4 dBm
	Mean channel launch power maximum				
	Type A link	+9 dBm	+9 dBm	+9 dBm	NA
	Type B link	+7 dBm	+7 dBm	+7 dBm	+9 dBm
	Minimum ER	6 dBm			
Receiver	*BER reference level*	10^{-3}			
	ODN class	N1	N2	E1	E2
	Sensitivity	-28 dBm	-28 dBm	-28 dBm	-28 dBm
	Overload	-7 dBm	-7 dBm	-7 dBm	-9 dBm

Table 2.5: Optical Interface parameters of the ONU for 10 Gbit/s. [11]

2.2.1.6 OLT Requirements

Similarly to ONU, in this section it will be presented the requirements for the OLT considering the same variables (ODN class, link type and bit rate). Again, the first table (Table 2.6) is referring to the 2.5 Gbit/s and the second one (Table 2.7) to the 10 Gbit/s.

Block	Parameter	Value			
Transmitter	*Nominal line rate*	2.48832 Gbit/s			
	Operating wavelength band	1596 - 1603 nm			
	Operating channel spacing	100 GHz			
	Line code	Scrambled NRZ			
	ODN class	N1	N2	E1	E2
	Mean channel launch power minimum	0 dBm	+2 dBm	+4 dBm	+6 dBm
	Mean channel launch power maximum	+4 dBm	+6 dBm	+8 dBm	+10 dBm
	Minimum ER	8.2 dBm			
Receiver	*BER reference level*	10^{-4}			
	ODN class	N1	N2	E1	E2
	Sensitivity				
	Type A link	-26 dBm	-28 dBm	-30.5 dBm	-32.5 dBm
	Type B link	-30 dBm	-32 dBm	-34.5 dBm	-36.5 dBm
	Overload				
	Type A link	-5 dBm	-7 dBm	-9 dBm	-11 dBm
	Type B link	-9 dBm	-11 dBm	-13 dBm	-15 dBm

Table 2.6: Optical Interface parameters of the OLT for 2.5 Gbit/s. [11]

Block	Parameter	Value			
Transmitter	*Nominal line rate*	9.95328 Gbit/s			
	Operating wavelength band	1596 - 1603 nm			
	Operating channel spacing	100 GHz			
	Line code	Scrambled NRZ			
	ODN class	N1	N2	E1	E2
	Mean channel launch power minimum	+3 dBm	+5 dBm	+7 dBm	+9 dBm
	Mean channel launch power maximum	+7 dBm	+9 dBm	+11 dBm	+11 dBm
	Minimum ER	8.2 dBm			
Receiver	*BER reference level*	10^{-3}			
	ODN class	N1	N2	E1	E2
	Sensitivity				
	Type A link	-26.5 dBm	-28.5 dBm	-31 dBm	NA
	Type B link	-28.5 dBm	-30.5 dBm	-33 dBm	-33 dBm
	Overload				
	Type A link	-5 dBm	-7 dBm	-9 dBm	NA
	Type B link	-7 dBm	-9 dBm	-11 dBm	-11 dBm

Table 2.7: Optical Interface parameters of the OLT for 10 Gbit/s. [11]

2.2.1.7 OLT and ONU common considerations

In Tables 2.4, 2.5, 2.6 and 2.7, "Type A link" and "Type B link" considerations are made for link types. These considerations assume:

- Type A link as an unamplified OLT receiver, although it is not prohibited the use of amplification;
- Type B link as an amplified OLT receiver with the amplifier at the S/R-CG reference point (Figure 2.4). Again, it is allowed other approaches, including the absence of amplified OLT;

The final consideration about the above mentioned tables, is about the ER. This value can be lower than it is described, however it must be compensated by a larger "Mean launch power maximum" value for the same tables [12].

Chapter 3

Photonic Integrated Circuits and its components

This chapter starts with a briefly state of the art where it is described the importance of photonic integrated circuits nowadays, as well as a first presentation of the foundries to be mentioned along this work (section 3.1). Next, a theoretical section about the several components that usually integrate this circuits (section 3.2), finishing with a software simulation of a system using these components in section 3.3.

3.1 Photonic Integrated Circuits

PICs are a multi-functional optical integration device similar to an electronic integrated circuit. The main difference is that PIC's signals are in wavelengths typically from visible spectrum, infrared up to 1650 nm.

These chips may encompass large range of components, including waveguides, couplers, optical modulators, filters, lasers, photodetectors, optical amplifier and so on. Besides that, the main advantages of PICs are the design simplification due to integration, the footprint reducement, the reliability improvement and, mostly, the possibility to decrease the number of Optical-Electrical-Optical (OEO) conversions [14].

One of the most used materials to fabricate these circuits is InP due to its viability for integration of active and passive functions in the same chip. Despite that, PICs were made using several different materials including electric-optical crystals such as Lithium niobate, silica over silicon, silicon over insulating among other polymers and semi-conductor materials as GaAs (Gallium Arsenide) and InP. Each one of these combinations have different advantages, disadvantages and limitations and for that reason the choice must be accordingly to the final function the PIC will provide [15].

Nowadays, the production of these chips can be done in MPW runs. These projects aggregate multiple chips from different clients in one single run, in order to minimize the production costs. Figure 3.1 presents a comparison table of materials and performance that this project commercially provides.

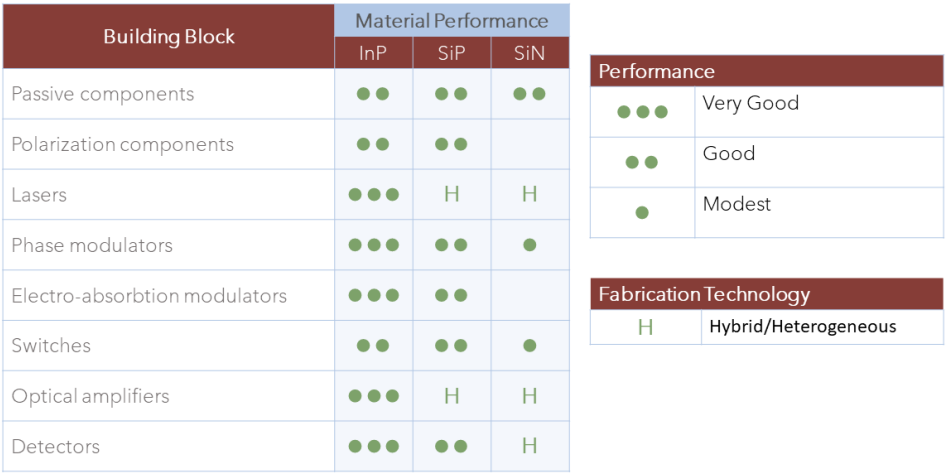

Figure 3.1: Performance comparison of the commercially available technology platforms. (Based on [19])

As it is possible to see in Figure 3.1, the overall performance of InP-based Building Block (BB)s present better results than TriPleX (SiP and SiN based BBs).

In [16], the two main foundries recommended for InP-based chips are SmartPhotonics and Fraunhofer Heinrich Hertz Institute (FhG-HHI).

Table 3.1 describes several building blocks from both foundries as well as their performance.

Component	*Specification*	*Foundry*	
		HHI	***SmartPhotonics***
Lasers and Amplifiers			
SOA	*Gain* *Saturation Power*	92 cm - I @ 7000 A/cm^2 13 dBm	70 cm - I @ 7000 A/cm^2 13 dBm
DBR grating	*Tuning range*	4 nm	1 nm (uniform, not optimized)
DFB laser	*Tuning range* *Output power* *Small signal bandwidth*	4 nm 10 mW @ 150 mA 20 GHz @ 100 mA	on request 10 mW @ 100 mA on request
DBR laser	*Tuning range*	4 nm	on request
	Output power	20 mW @ 150 mA	10 mW @ 100 mA
Isolation Section		yes	yes
Broad band reflectors			
1x2 MMI reflector	*Loss*	*	2 dB
	Reflectivity		40 %
1x1 MMI reflector	*Loss* *Reflectivity*	*	2 dB 70 %
Polarization devices			
Polarization splitter	*Loss*	2 dB	*
	PER	25 dB	
Polarization converter	*Loss*	1 dB	*
	PER	20 dB	
PIN photodiode			
	3 dB bandwidth	45 GHz	18 GHz (RF pin diode) / >25 GHz on request
	Dark current	2 nA @ -2 dV	<25 nA @ -2 V Bias (DC pin diode)
	Sensitivity	0.8 A/W	0.85 A/W
Modulators			
Thermo-optic phase modulator	*Loss*	2 dB/cm	*
	I(PI) x L	20 mA x mm	
Current injection phase modulator	*Loss*	2 dB for 100-200 um	<0.5 dB for 2 mm
	I(PI) x L	20 mA x mm	t.b.d.
Electro-Optical phase modulator	*Loss* *Bandwidth* *U(PI) x L*	coming with HHI19, expected loss 4 dB expected value 30 GHz expected 4 V	<0.5 dB for 2 mm 15 GHz Vpi = 5V
Electro-Absorption modulator	*EO bandwidth*	20 GHz	
	ER/ length	10 dB / 100 um	
Spot size converter for edge coupling			
		Available. Loss waveguide to SSMF is 1.5 dB	lateral taper
Passive waveguides			
Straight waveguide	*Loss*	<2 dB/cm	2 dB/cm
Arc waveguide	*Minimal radius*	150 um	100 um
Tapered waveguide	*Loss*	2 dB/cm	2 dB/cm
Couplers			
1x2 MMI coupler	*Loss*	0.5 dB	0.5 dB (typical), max 1 dB
Directional coupler	*Loss*	0.5 dB	
* Building Blocks under development			

Table 3.1: Latest capability overview over the building blocks for PIC's fabrication InP based in MPW run. (Based on [19])

As it is possible to see in Table 3.1, both foundries have their respective specifications and particularities for each BB, including differences in the available structures. This will take

part as the designing process of the chip, once it is necessary to be profoundly aware of the chip final purpose and how it will be implemented, in order to fulfill those necessities and requirements. Then, the foundry choosing process must concern the BB available from both foundries, as well as their specifications, for a final implementation that correctly fulfills the chip requirements and objectives.

Both foundries provides also different cell sizes (total area occupied by the PIC) and number of reproductions. In FhG-HHI, it is possible to get a 4 chip copies for 3 different sizes: 2 x 6 mm^2, 4 x 6 mm^2 or 12 x 6 mm^2 of total design area. While SmartPhotonics allows the production of 8 copies of the chip but only for 2 available areas: 4 x 4.6 mm^2 and 8 x 4.6 mm^2 of total design area [16].

Concluding, the development process of a PIC it is divided into several steps forming a design flow [16]:

1. Analyse and choose the foundry that most meets the final demands of the chip;
2. Develop the PIC architecture accordingly to its requirements and application, using the appropriate BBs available from the chosen foundry;
3. Confirm the final layout with the Design Rule Check tests for ensuring the correct implementation of the manual rules;
4. Check the MPW run schedule and apply for a run;
5. Submit the design.

After receiving the chip, it is necessary to perform several laboratory tests to ensure the PIC's correct fabrication and performance.

3.2 Optical components

Similarly to integrated electronics, at optical communications there are also optical integrated circuits where several necessary components are integrated for the most different systems implementation and functionalities. As shown in Figure 3.1, it is possible to find some active components such as: lasers, modulators, optical amplifiers and photodetectors but also several passive elements such as couplers, filters, multiplexers and demultiplexers.

3.2.1 Light Sources and modulation

The radiation mechanisms in a semiconductor are characterized by the type of movement electrons realize: spontaneous emission, stimulated emission and stimulated absorption [17].

Primarily, it is possible to distinguish an absorption from an emission through the energy level that the protagonist electron leaves relatively to the one it goes. Therefore, if the electron realizes a level growth, namely, it goes from a low energy level to a higher energy level, the process is called absorption and, consequently, the inverse process is called emission [17].

As referred before, there are two different types of emission: spontaneous and stimulated. Spontaneous emission illustrated by Figure 3.2 b), occurs when, such as it name suggest, spontaneously, an electron allocated in a high-energy level loose energy and dive into a lower energy level. If the difference between these energy levels is lower than the energy absorbed

by the electron, it is generated a photon from this process. The resulting light is incoherent and random what makes it non ideal to use in optical communications [17].

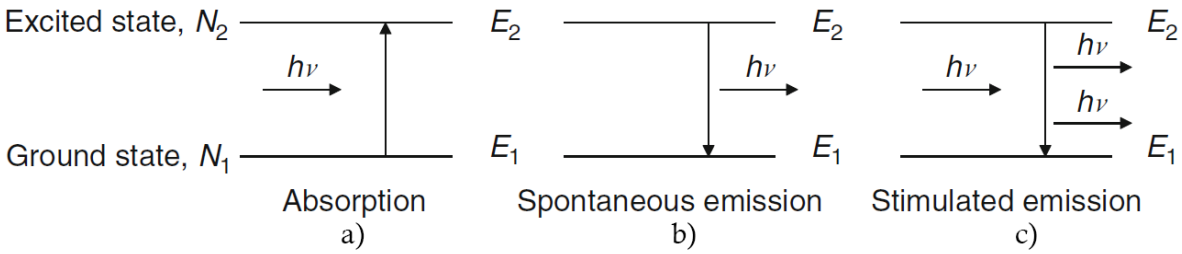

Figure 3.2: Schematic of the three main light processes: a) absorption, b) spontaneous, c) stimulated emission. [19]

In the same Figure 3.2 c), it is described a stimulated emission. This process occurs when a photon with enough energy acts on the semiconductor and causes a stimulated recombination between a conduction's band carrier and a valence's band hole, producing one photon with similar energy to the originating one. The resulting light is coherent, since photons that originate it have the same frequency and direction characteristics as the one resulting from the process [17].

To achieve higher stimulated emission than spontaneous emission, it is necessary to guaranty the population inversion. This condition means that there are more electrons on the higher energy levels than in the ground level. To guarantee that, it is required enough pumping [18]. The dependency between light output power and the current injected is illustrated in Figure 3.3. [19].

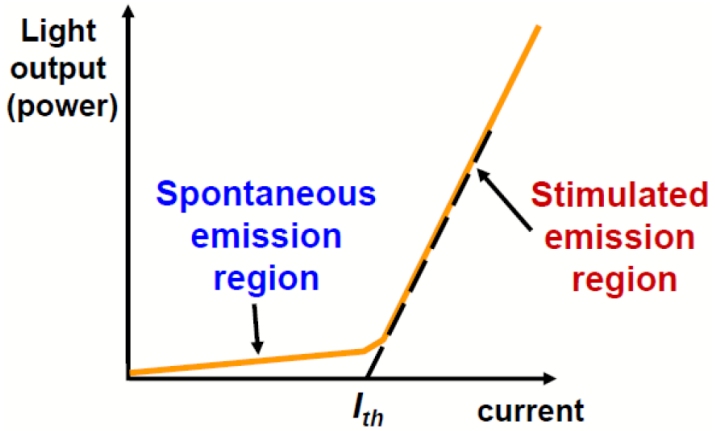

Figure 3.3: Light output power as a function of injected current. [5]

As it is possible to see in Figure 3.3, there is a threshold current I_{th} value for which the type of produced light is dependent on. For injected current below this value, the output light results in spontaneous emission and therefore not relevant because of its non-coherent properties and low power. On the other hand, when the injected current is above the threshold value, the output light power increases steeply with the current produced by stimulated emission with coherent light.

3.2.1.1 Distributed Feedback Laser

DFB lasers are the most common light source used in telecommunications industry, mostly due to its tunability. They have also several beneficial characteristics to optical communications such as narrow linewidths, low chirp effect, low relative intensity noise and potential high bit rate useful for long transmission distance [17] [20].

Figure 3.4 illustrates a DFB structure.

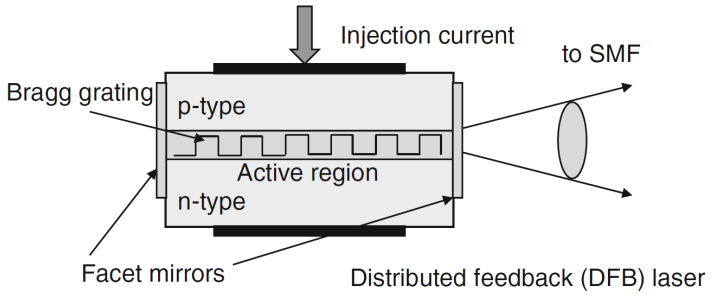

Figure 3.4: DFB Laser structure. [19]

As it is possible to see in Figure 3.4, it has two facet mirrors at both ends and in between, it is composed by an active region, top and bottom contoured by a p and n-type layers, respectively. The pumping applied to these devices to achieve the population inversion, is electrical.

The feedback mechanism takes place in the cavity region, where it is possible to find a Bragg grating. This grating leads to a periodical variation of the waveguide refractive index, which will then create a propagation of coupled waves in both directions (forward and backwards). The working mode selection is dependent on the refractive index variation period and the average mode index [21].

The electrical pumping used to achieve population inversion, beyond the addiction of gain, indirectly allows the tunability of this device. The current injection into the laser, acts as an internal resistor and increases its temperature. Also, this thermal process, changes the volume of the grating cavity, leading the refractive index to change and resulting in wavelength tunability [21].

Being familiar with the emission process, it is important to be aware also of the modulation processes, which are crucial in transferring data procedure. The two main modulation types are direct and external modulation. These techniques need to fulfil several requirements such as:

- ***Speed of operation***: both external and direct modulation must be able to switch between high and low level states within a fraction of bit duration for a specific bit rate;

- ***Extinction ratio***: the ER of the optical signal is defined as

$$\mathrm{ER} = \frac{P_1}{P_0} \tag{3.1}$$

  where P_1 and P_0 are, respectively, the power levels for the high and low bits, so it describes the separation between the power of the two values [22].

3.2.1.2 Direct Modulation

In direct modulation, there is no external modules and the laser itself is capable to modulate the radiant output power by turning the light on and off through the injected current creating an On-Off Keying (OOK) signal [22]. A schematic of this modulation is presented in Figure 3.5 .

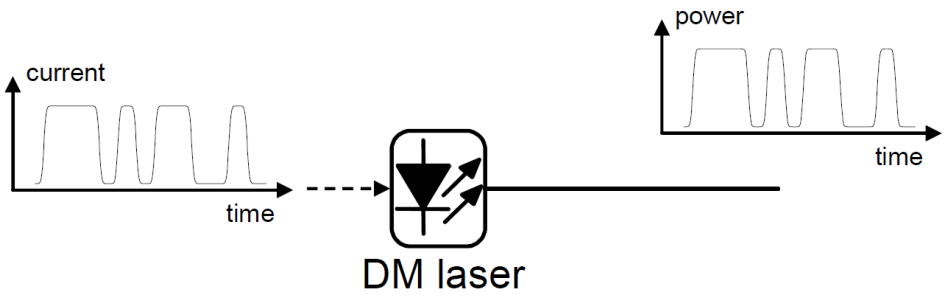

Figure 3.5: Direct modulation diagram. [21]

The main advantage of this type of lasers is their design simplicity and low price, however are not preferred when compared to External Modulated Laser (EML) due to its lower performance at high bit rates. Other characteristics associated to direct modulation are distortion, low ER and chirp effect [22].

3.2.1.3 External Modulation

External modulation schematic is represented in Figure 3.6 [18][22].

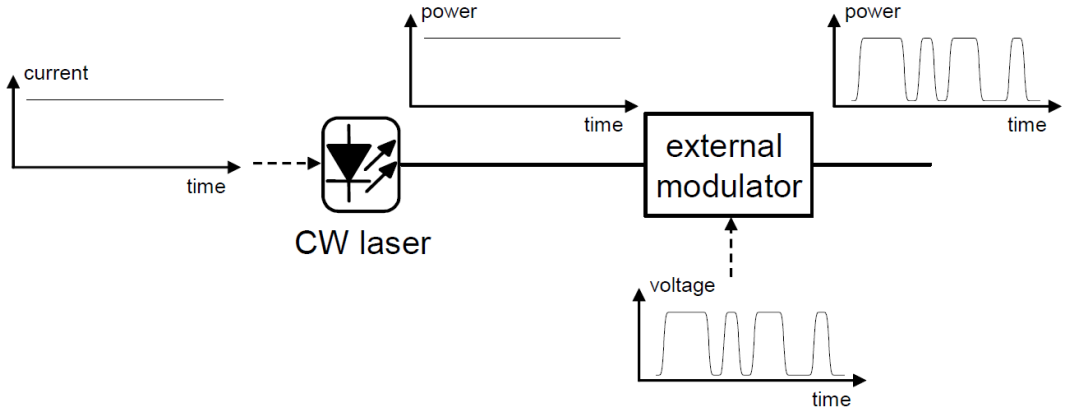

Figure 3.6: External modulation diagram. [21]

The main difference between the Direct Modulated Laser (DML) and EML, is the fact that in this case, the laser operates in a Continuous Wave (CW) regime leaving the modulation to an external block and allowing the possibility to optimize the output power and control independently the ER [18][22].

There are two types of external modulators most commonly used in optical communication systems: electro-absorption modulators and electro-optic modulators.

The electro-absorption modulators operating mode is based on the effective bandgap dependence on the external voltage applied. When no voltage is applied, if the energy of the incoming light is smaller than the bandgap energy value, the material will be transparent, and no absorption effect occurs. On the other hand, by applying an external voltage to the material, the effective bandgap will be reduced and, for input light energy values higher than the bandgap's energy, absorption will take place in the semiconductor's material. The variation of absorption accordingly to the wavelength for both presence and absence of external voltage is represented in Figure 3.7[22].

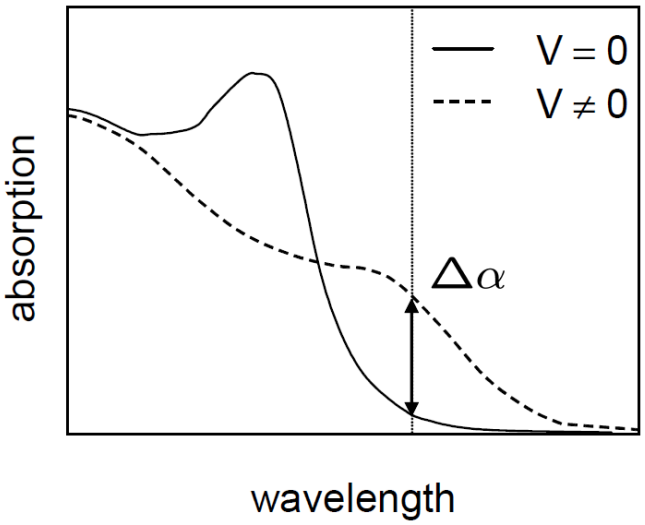

Figure 3.7: Absorption of a semiconductor as a function of wavelength with and without external voltage applied. [21]

As it is possible to see in Figure 3.7, by properly selecting the input wavelength, it is possible to experience a significant variation in absorption when the voltage is applied, it thus becomes possible to achieve optical intensity modulation controlled by the electrical signal (the external voltage applied). However, the absorption shifting will induce a change in the Refractive Index (RI) of the semiconductor material changing the input signal's phase. Consequently, some frequency chirp will be introduced, although it usually is much lower than direct modulation [22].

On the other hand, there are the electro-optic modulators where the refractive index of some materials change when applying an external electric field to them. The applied voltage will modulate the refractive index of the waveguide material resulting in the phase change of the lightwave propagating along the waveguide, and phase modulation [22].

3.2.2 Optical Fiber

Optical fiber is a waveguide made of high-purity glasses. The cylindrical core of a fiber has a slightly lower RI than the cladding surrounding it. Light enters in one end of the fiber and travels confined within its core, along all its length, until it reaches the other end. Optical fibers can be classified as Single Mode Fiber (SMF) or Multi Mode Fiber (MMF) accordingly with the core diameter: for diameter values large enough to propagate multiple modes, the optical fiber is classified as MMF and for smaller values, it is only possible to propagate one mode, therefore, it is called SMF [9].

Along optical fiber's length, a little part of that light is lost [17]. This happens because optical fiber has loss. Also, dispersion processes are present and may cause great impact in transmission capacity and limits the maximum distance.

3.2.2.1 Fiber loss contributions

Loss processes are mainly absorption, scattering and bending, being absorption the most impacting factor. When propagating through optical fiber structures, light pulses will became

weaker due to absorption process of impurities in the glass [17].

Therefore, the mathematical relation between the input optical power introduced into a fiber with length L and its output optical power, considering the absorption impact, is described by

$$P_{out}(L) = P_{in} \cdot e^{-\alpha L} \tag{3.2}$$

where α is the attenuation coefficient, P_{in} the input light power and P_{out} the output light power. By 3.2, it is possible to see that, for an ideal glass without impurities ($\alpha = 0$) the output power is equal to the input power without any dependency with the propagation length. However, the biggest the absorption coefficient gets, the most the output power will become.

The origin of the attenuation coefficient can have intrinsic or extrinsic sources, of which impurities stand out. This factor changes the cladding RI and affects the full reflection. In fact, the major contribution to the optical communications development was the discovery of the relation of this parameter with the propagation wavelength. By 1970, silicon fibre attenuation was 20 dB/km due to the wavelength used. In 1990 the attenuation becomes 100 times smaller (approximately 0.2 dB/km) when it was used for the first time an operating wavelength near of 1.3 and 1.5 μm [17].

3.2.2.2 Dispersion

Dispersion occurs when light propagating through optical fiber gets spread out. When a short pulse becomes longer, the possibility to join with the previous pulse increases resulting in an increased probability of recovery error in reception [17]. Figure 3.8 shows the ISI caused by dispersion.

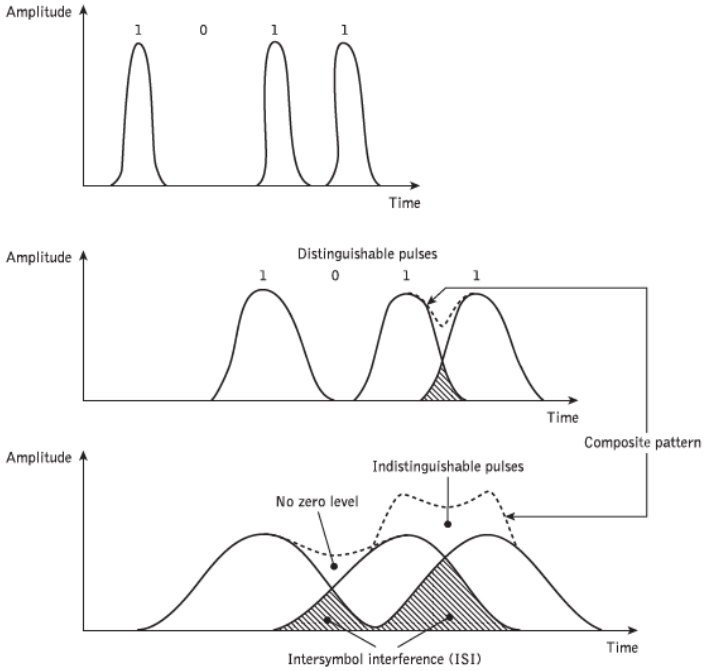

Figure 3.8: Illustration of the dispersion effect in light pulses causing ISI. [6]

The main types of dispersion are: the chromatic dispersion and the modal dispersion.

The first one is caused by the spectral width of the light source. Both Light Emitting Diode (LED)s and lasers produce a range of optical wavelengths rather than a single narrow wavelength, and, as it is known, optical fibre's RI varies with wavelength and, for that reason, each wavelength injected by the light source will travel at a different speed in the fibre. On the other hand, there is the modal dispersion associated to the many paths that light travels through the fiber [17].

The chromatic dispersion parameter is represented by D in ps/nm·km. This parameter is used to estimate the transmission limit of optical fiber imposed by dispersion using

$$\Delta t = \Delta t_{cro} = |D| \cdot L \cdot \Delta\lambda_{source} < \frac{1}{B} \tag{3.3}$$

, considering L the transmission limit (km), $\Delta\lambda_{source}$ the wavelength (nm) and B(bits/s) the transmission rate.

Depending on the type of fiber, the dominant effect will vary: for SMF there is no intermodal dispersion, so the dominant effect will be chromatic dispersion, and, for Step Index Multimode Fiber (SI-MMF), the dominant effect will be intermodal dispersion. At last there is Graded Index Multimode Fiber (GI-MMF) where no factor is dominant. This reduction of intermodal dispersion relatively to step-index multimode fibers results in higher bandwidth [21].

3.2.3 Semiconductor Optical Amplifier

Similarly to the electric circuit's power amplifier, there is also a component in optical circuits responsible to amplify the signal. Besides that, SOA also provides wide spectral bandwidth. This component uses a semiconductor to provide the signal amplification.

The structure of a SOA is provided in Figure 3.9.

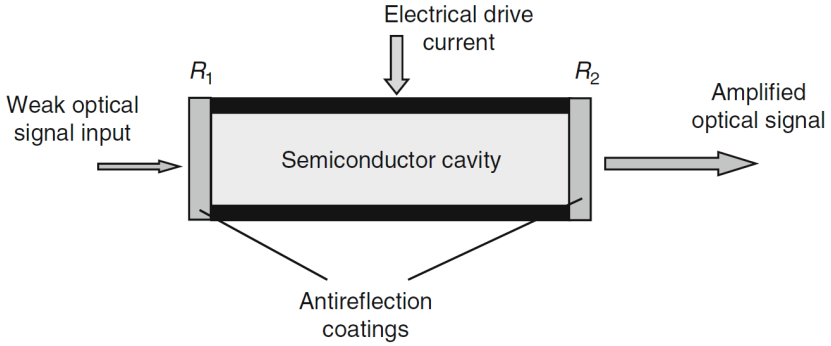

Figure 3.9: SOA structure and operation principle. [19]

The operational principle of this component is similar to distributed feedback lasers and it is based on its structure and an external injection of current. Once the input signal goes through the active region, that external energy source enables pumping electrons to the conduction band. This causes electron's transition from the conduction to the valence band, emitting a coherent output light, feature of stimulated emission [18] [21].

The gain provided by the pumping of electrons through external current will also amplify the optical noise caused by the spontaneous emission that occurs through the SOA. In order to reduce this phenomenon and to increase the available carrier population for optical gain,

the injected current to the SOA needs to be sufficiently high to create a maximum population inversion [21].

In Figure 3.10 a) and c), it is possible to see that light in Fabry-Perot SOAs suffers different partially reflections thanks to the reflective facets at the edges of the device, while Travelling-wave SOA (Figure 3.10 b) and d)) contains anti-reflection coatings which makes the light propagate only once in the gain surface [23].

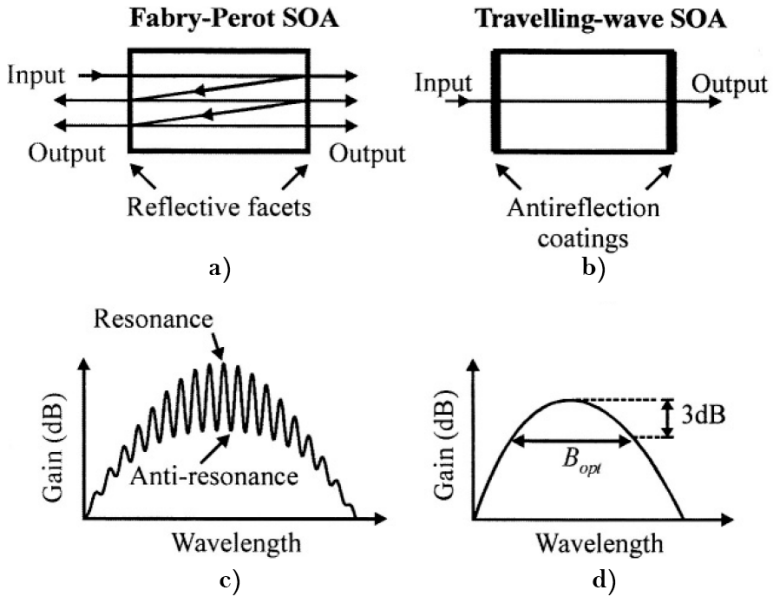

Figure 3.10: SOA types: a)Fabry-Perot SOA structure, b)Travelling-wave SOA structure, c) Gain spectrum performance of FP-SOA, d) Gain spectrum performance of TW-SOA. [22]

In Figure 3.10 c) and d) it is also possible to see how the gain behaves along the wavelength spectrum in both structures.

In FP-SOA the partial reflections produce ripples in its gain spectrum similarly to a resonant effect. In TW-SOA the gain becomes smoother, making the resulting gain of the first one, more sensitive to variations in bias current, temperature and signal polarisation. Moreover, TW-SOA's bandwidth is wider than the resonant amplifier (FP-SOA) and higher saturation power. It also reduces the temperature and current density, making this one the more desirable and used structure nowadays [23].

The main feature of this component is then the gain that it is capable to introduce to the signal, which is defined by the ratio between the output optical power and the input optical power.

In Figure 3.11 it is possible to see the dependency of a SOA gain as a function of the output power.

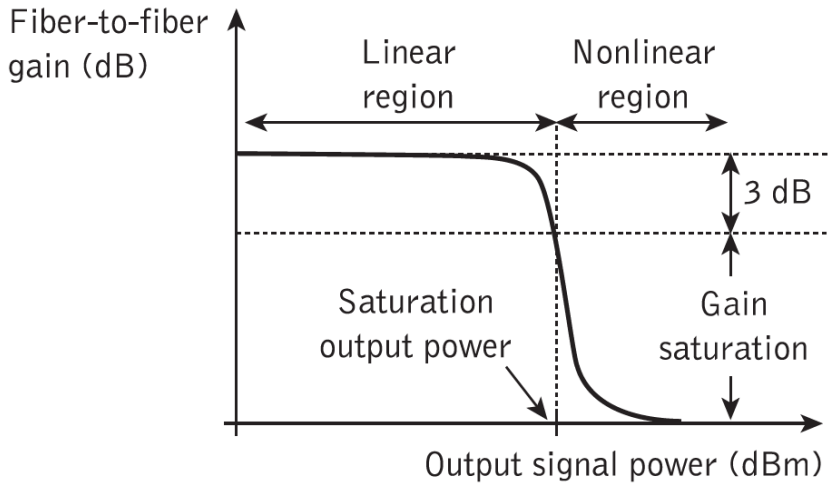

Figure 3.11: Typical fiber-to-fiber gain against output signal power characteristic. [7]

The gain behaviour described in Figure 3.11 shows that, for smaller output signal power, there is a flat linear region where the SOA achieves the maximum gain without non-linear effects.

For higher output power signals, saturation gain region is reached. This happens when there are no more carriers available in the active region of the SOA structure, and the gain value falls. When the input power increases too much and the gain reaches the saturation region, the behaviour of the amplifier is no longer linear and drops drastically.

In linear region, there are other two factors that influence the maximum gain the SOA may achieve and they are the bias current and the wavelength. For larger bias the optical output power increases and its maximum gain value varies for different values of wavelength [6].

In sum, SOA is a key element in PIC technology and optical communications offering large gain, large optical bandwidth, very short response times, compact structure prone for integration and low price. The different applications of this device are also an important factor once they vary accordingly to its relative position to other components. In the transmission part it can increase the power of the signal transmitted, allowing the loss of power through the length of the network without losing completely the signal. In the reception part it can increase the signal power before it is received by the photodetector, improving the sensitivity.

3.2.4 Photodetector

Photodetector's main function is to convert optical signals into electrical. In order to fulfil optical communications requirements, these components must be chosen according to several basic requirements such as high sensitivity at the required wavelength and bit rate (low capacitance with a fast response), low noise, high reliability and low cost [24].

When an incident photon has energy greater than the bandgap of a semiconductor material, its energy will be absorbed, and an electron is excited from the valence to the conduction band generating a hole in the valence band. The electric field generated creates a separation between holes and electrons which result in an electrical current generation. Equation 3.4 describes the proportionality between the generated current and the incident optical power

$$I_p = R \times P_{in} \tag{3.4}$$

where I_p is the current generated in the photodetector, P_{in} is the optical power injected and R is responsivity measured in units of A/W. This last parameter is, as mentioned before, one of the most relevant ones in the process of choosing a photodetector. Responsivity defines the ratio between the two parameters referred (current and injected power). The mathematical definition of this parameter is expressed by

$$R = \frac{q\eta}{hf} \tag{3.5}$$

where q is the electron charge, h the Planck's constant, f the photon frequency and η the quantum efficiency, which represent the ratio between the number of generated electrons per number of incident photons [24].

Despite that, a photodetector's responsivity is affected by many factors such as wavelength of the incident light, the bias voltage applied and the temperature.

Considering wavelength, an ideal photodetector describes a linear proportionality between responsivity and wavelength due to the increasing number of photons for the same optical power, but in typical photodetector the responsivity increases with wavelength until a certain point where the quantum efficiency drops to almost zero due to the photon energy, becoming too small to generate any electron. This point is also dependent on the material that is being used for semiconductor and it is commonly called the cut-off wavelength value. This behaviour is possible to see in Figure 3.12 for multiple materials [24].

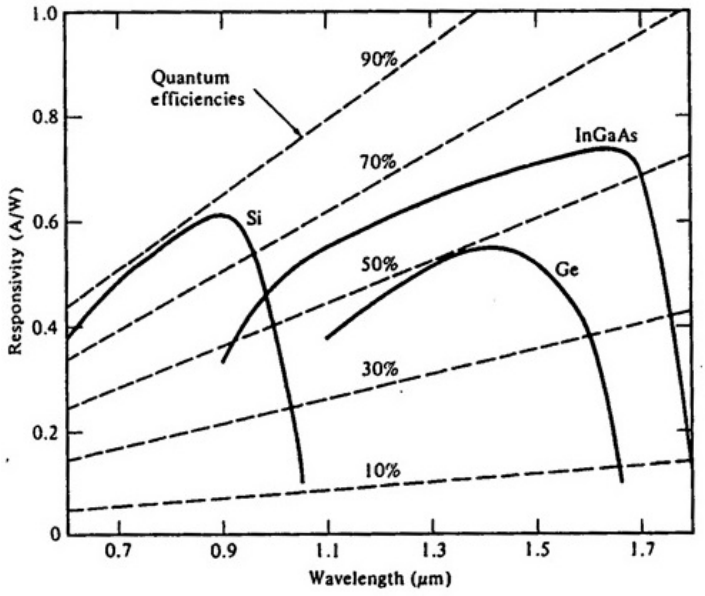

Figure 3.12: Responsivity of several semiconductor materials as a function of the wavelength. [24]

3.2.4.1 Most common photodetector: p-i-n

There are many different photodetectors types, being the most commonly used the p-i-n photodiode and, for that reason, it is described in this subsection.

A simple structure of a p-i-n photodiode is described in Figure 3.13.

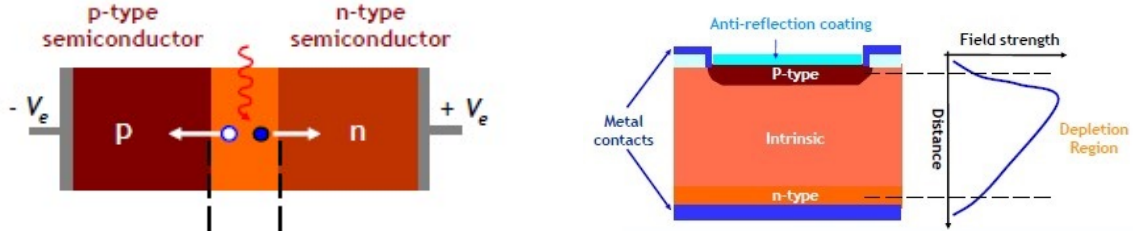

Figure 3.13: a) PIN structure b) PIN structure and its electrical field distribution. [5]

As it is possible to see in Figure 3.13, the structure of a p-i-n photodiode (PIN) is composed by a p type and a n type layer, with an intrinsic layer between them. Due to its intrinsic nature, the middle intrinsic layer offers a high resistance, and, for that reason, a substantial voltage is dropped when crossing this layer [21].

The presence of this intrinsic region makes it possible for the photodetector to increase the depletion region width, the absorption of the incident light and also its quantum efficiency [21].

3.2.4.2 Photodetector noise mechanisms

In optical receivers there are two sources, besides others, of noise mechanisms: electric shot noise and thermal noise.

The electric shot noise is a manifestation of the fact that an electric current consists of a stream of electrons that are generated at random times[21]. Its value is given by

$$< i_{shot}^2 >= 2 \cdot q \cdot I \cdot B_e \tag{3.6}$$

where q is the electron charge, I is the photocurrent and B_e is the electrical bandwidth.

Thermal noise is the result of thermally induced random fluctuation in the charge carriers in a resistance and it has relevant values even when no voltage is applied through the resistance. The thermal noise mean square is given by

$$< i_{ther}^2 >= \frac{4k \cdot T \cdot B_e}{R} \tag{3.7}$$

Where k is the Boltzmann's constant, T is the resistance temperature and R is the resistance value.

- Bit error rate

  The addiction of noise generates errors in the detection process. This originates BER which can be calculated using

  $$BER = \frac{n_e}{n_{total}} \tag{3.8}$$

  where n_e is the number of bits detected incorrectly and n_{total} is the total number of bits transmitted. It also can be tested using a BER test set where errors are counted when comparing the received sequence and the original one.

  This parameter can also be estimated by Error Probability (PE). Considering two-level modulation, the error probability estimation considers a noise distribution on the

high and the low bit level (bit 1' and 0') but also their average value and variance. Figure 3.14 illustrates graphical '0' and '1' levels with the according average and variance distributions.

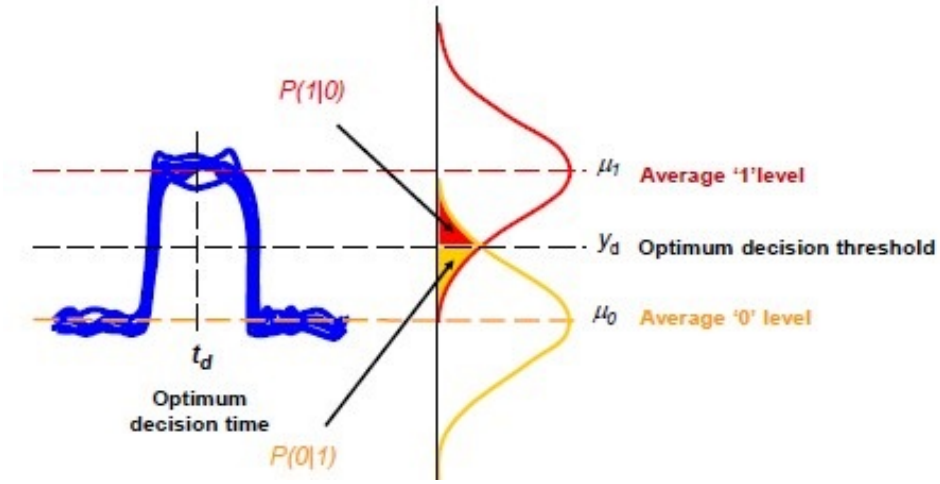

Figure 3.14: Error Probability estimation for two-level modulation. [5]

In Figure 3.14 it is possible to see the graphical illustration of the probability of detecting '0' when a '1' bit was sent and vice versa. This probability is then used to calculate the PE using

$$\text{PE} = p(1) \cdot P(0 \mid 1) + p(0) \cdot P(1 \mid 0). \tag{3.9}$$

The signal's quality can also be estimated by the Q factor when the '1' and '0' mean levels and their noise powers are known for the specific signal. Q factor can be calculated using

$$Q = \frac{\mu_1 - \mu_0}{\sigma_0 + \sigma_1}. \tag{3.10}$$

wich is also related with BER by

$$\text{BER} = \frac{1}{2} erfc(\frac{Q}{\sqrt{2}}) \tag{3.11}$$

.

The variation of BER with the Q parameter is described by Figure 3.15 where it is plotted a MATLAB illustration of Equation 3.11.

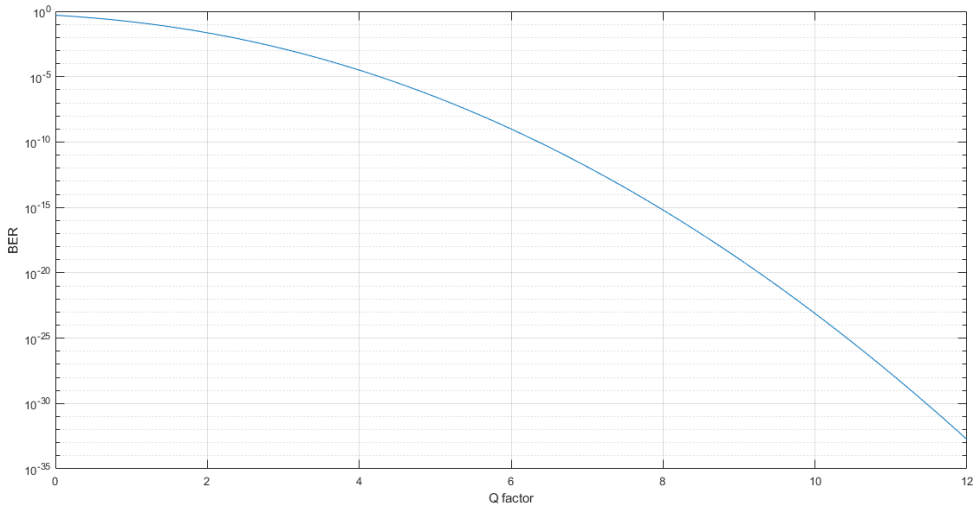

Figure 3.15: BER versus the Q parameter.

3.3 Simulation of modulation types

In this section simulations of system implementations as well as performance analysis of the components studied on the previous sections using Lummerical's tool INTERCONNECT will be presented.

3.3.1 External modulation

In Figure 3.16 is demonstrated the setup used to test the direct modulation in INTERCONNECT.

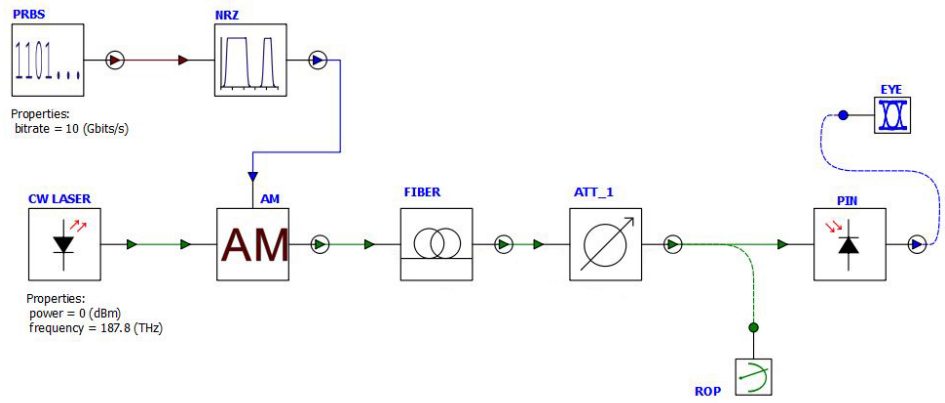

Figure 3.16: Setup used to test external modulation format for different fiber lengths and received optical power.

It begins with a digital binary random source that generates a 1024 bit logic sequence

connected to a NRZ block that transforms this sequence into an electric signal that will be one of the sources for the Electro-Absorption Modulator (EAM) block presented next. The modulator also receives an optical signal from a CW laser with, in the present case, 0 dBm of output power.

The external modulation block is then connected to a linear fiber block with length varying between Back-to-Back (B2B) (0 km), 10 km and 20 km. Fiber dispersion and attenuation parameters is, respectively, set as 16 ps/(nm·km) and 0.2 dB/km. The signal is then connected to a PIN with a responsivity value of 0.8 A/W, and then connected to an electric eye diagram block to calculate the Q-factor value, an optical power meter between the attenuator and the photodetector to measure the Received Optical Power (ROP).

The operating frequency chosen was the first channel frequency in L band (187.8 THz) at a 10 Gbit/s bit rate which is according to NG-PON2 requirements.

The complete description of these blocks parameters is listed in Table 3.2

Block	***Parameter***	***Value***
PRBS	Bit rate	10 GBit/s
NRZ	Amplitude	1
	Bias	0
	Rise period	0.05
	Fall period	0.05
CW Laser	Frequency	187.8 THz
	Power	0 dBm
	Linewidth	0 MHz
	Phase	0 rad
AM modulator	Modulation index	1
Optical Fiber	Length	[0; 10; 20] km
	Configuration	unidirectional
	Reference Frequency	187.8 THz
	Attenuation	0.2 dB/km
	Dispersion	16 ps/(nm·km)
	Dispersion slope	0.08 ps/nmˆ2/km
Attenuator	Configuration	unidirectional
	Attenuation (B2B/ 10 km/ 20 km)	[16; 30]/ [14; 28]/ [12; 26] dB
PIN	Frequency at max power	true
	Responsivity	0.8 A/W
	Dark current	1e-8 A
	Thermal noise	1e-13 A/Hzˆ.5
	Enable power saturation	false
	Enable thermal noise	true
	Enable shot noise	true
	Enable noise bins	true
	Automatic seed	true

Table 3.2: Full parameters description of the implemented blocks in setup from Figure 3.16.

- Results

  The simulations were focused in evaluating the Q-factor of the signal received in the photodetector when varying the attenuation values for the different fiber length values. The results are presented in Figure 3.17.

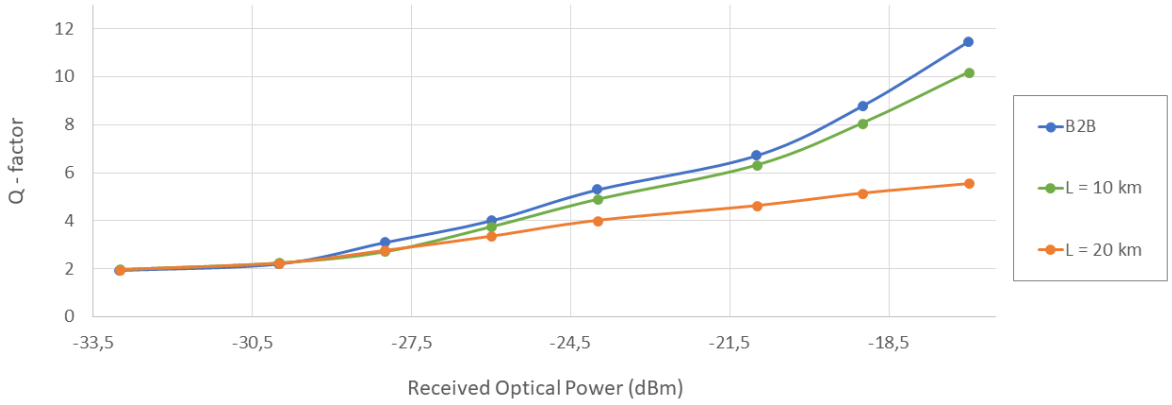

Figure 3.17: Variation of Q-factor for multiple fiber lengths when varying the received optical power by the PIN for external modulation.

As it is possible to see by Figure 3.17, the Q-factor values are higher for higher ROP. Also, the longer the fiber, greater becomes the degradation of Q-factor for the different attenuation values.

3.3.2 Direct modulation

Direct modulation was also simulated at Lumerical's INTERCONNECT. The setup implemented is illustrated in Figure 3.18.

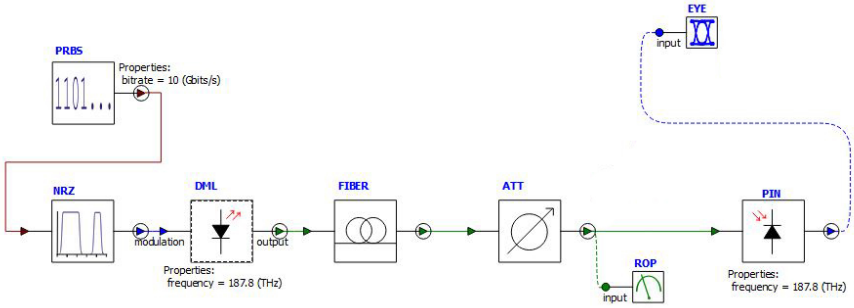

Figure 3.18: Setup used to test direct modulation format for different fiber lengths and received optical power.

Similarly to what was done for the external modulation setup, similar parameters were chosen (frequency of 187.8 THz and bit rate 10 Gbit/s). The first block is, again, a random generator logic bit sequence next to a NRZ block but, this time, the signal resulting from

this block is directly connected to a directly modulated laser. The optical signal produced presents the same ER as the obtained for the EML. Next it is connected to a linear fiber with lengths B2B(0 km), 10 km and 20 km with the same dispersion and attenuation parameter values as in the previous simulation, an attenuator and a PIN.

The complete description of these blocks parameters is listed in Table 3.3.

Block	***Parameter***	***Value***
PRBS	Bit rate	10 GBit/s
NRZ	Amplitude	1
	Bias	0
	Rise period	0.05
	Fall period	0.05
DM Laser	Frequency	187.8 THz
	Total quantum efficiency	0.0028
	Active volume	1.5 eˆ-16 mˆ3
	Mode confinement factor	0.4
	Spontaneous emission factor	3e-5
	Photon lifetime	3e-12 s
	Carrier Lifetime	1e-9 s
	Gain compression factor	1e-23 mˆ3
	Gain coefficient	2.5e-20 mˆ2
	Carrier density at transparency	1e+24 mˆ-3
	Linewidth enhancement factor	5
Optical Fiber	Length	[0; 10; 20] km
	Configuration	unidirectional
	Reference Frequency	187.8 THz
	Attenuation	0.2 dB/km
	Dispersion	16 ps/nm/km
	Dispersion slope	0.08 ps/nmˆ2/km
Attenuator	Configuration	unidirectional
	Attenuation (B2B/ 10 km/ 20 km)	[16; 30]/ [14; 28]/ [12; 26] dB
PIN	Frequency at max power	true
	Responsivity	0.8 A/W
	Dark current	1e-8 A
	Thermal noise	1e-13 A/Hzˆ.5
	Enable power saturation	false
	Enable thermal noise	true
	Enable shot noise	true
	Enable noise bins	true
	Automatic seed	true

Table 3.3: Full parameters description of the implemented blocks in setup from Figure 3.18.

- Results

  Using "sweep parameter"'s option from Lumerical's INTERCONNECT tool, ROP was varied. The resulting graph of this sweep is presented in Figure 3.19.

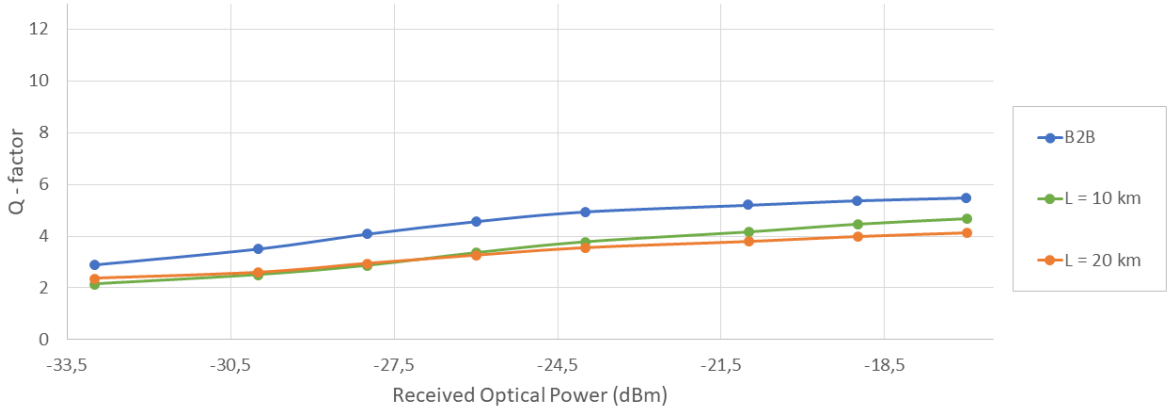

Figure 3.19: Variation of Q-factor for multiple fiber lengths when varying the received optical power by the PIN for direct modulation.

3.3.3 Comparison of results and conclusions

As it is possible to see for the both resulting graphs of external (Figure 3.17) and direct modulation (Figure 3.19) Q-factor performance, there is a clear difference behaviour. External modulation presents Q-factor values, for the same optical power received by the photodetector, much higher than the direct modulation system. The maximum Q-factor reached by direct modulation is near to 6, while external modulation reaches this value in the middle of the range of evaluation, reaching, for the maximum power values a Q-factor higher than 10. As it is possible to see in Figure 3.15, a Q-factor < 6 represents, for gaussian noise, a BER$> 10^{-9}$, while external modulation Q-factor results, according with Figure 3.15, is possible to present a BER $< 10^{-12}$, so, introducing less error to the system.

A general view on the results of both modulation techniques, allows to conclude that, for higher ROP, the higher the signal quality will be. However, it is expectable that direct modulation presents a lower performance due to the impact of the chirp effect in signals quality.

To conclude, between the margins for optical power reaching to the receiver established by [12] for NG-PON2, external modulation presents better performance than direct modulation, as it was expected by the theoretical analysis section in 3.2.1.

Chapter 4

Multimode Interferometer

This chapter is divided into two parts: the multimode interferometer structure and working principle and then the designing procedure of two 1x4 MMI couplers for the first four channels of the C and L bands. Firstly it is presented the basic structure of a MMI as well as its main advantages and the description of the self-imaging model for multimode interference. The designing part is then presented in section 4.2 where it is possible to see a full procedure description as well as the performance of the proposed designs.

4.1 Multimode Interference

The MMI device based on the self-imaging principle is an integrated optic component for PICs. This device has experienced, in the last years, a growing interest in its applications due to its characteristics of fulfilling several optical communications requirements such as: flexibility, reconfigurability, signal routing and coupling effect with large optical bandwidth and polarization insensitive in wavelength demultiplexing, but also its small dimensions and improved fabrication tolerances desirable for reducing process costs of PICs fabrication [25]. This device's structure can be divided in two main blocks: the access waveguides and the multimode waveguides. In Figure 4.1 it is possible to see a general representation of this structure.

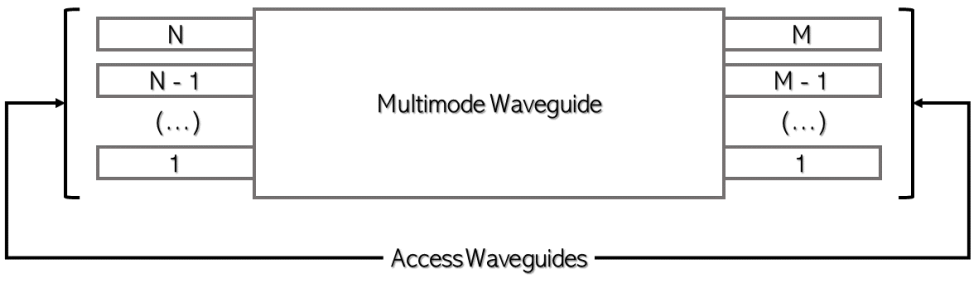

Figure 4.1: MMI general structure.

The input access waveguides launches light into the main section of this device (the multimode section) and the output recovers the light from it, both propagating in single mode. The central section, the multimode waveguide, is excited by the input segments and is able to propagate several modes [25].

These devices have numerous applications such as power splitters, ring lasers, optical couplers, optical switches, etc, and the amazing capacity to provide a wide range of N x M coupling functions with low insertion losses and a good balance between ports [25].

4.1.1 Multimode Waveguide Propagation

The Self-imaging principle where these devices are based on, is described as a "*property of multimode waveguides by which an input field profile is reproduced in single or multiple images at periodic intervals along the propagation direction of the guide*" [25] . Soldano et al. described in [25] the full-modal propagation analysis as the best way to describe this property using guided-Mode Propagation Analysis (MPA).

Considering a multimode waveguide constituted by a ridge and a cladding with effective RI, n_r and n_c (being $n_r > n_c$), respectively, and a ridge width W_M. In Figure 4.2 it is possible to see, considering z-axis as the propagation direction, the multiple reproduced field as single or multiple images through this structure.

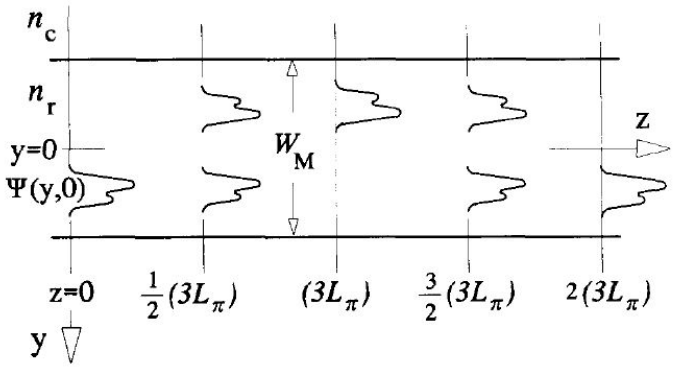

Figure 4.2: Multimode section with the input field $\Psi(y, 0)$ and mirrored images along its length. [25]

In Figure 4.2, along z-axis, it is possible to see single images of the input field $\Psi(y, 0)$ (for $z = 3L_\pi$ or $6L_\pi$) as well multiple reproductions of the same input (for $z = \frac{3}{2}L_\pi$ and $3L_\pi$), where L_π is the beat length of the two lowest-order modes. These points are caused by destructive and constructive interference of reflected modes propagating in the multimode section causing interference between them.

Although it may seem randomly, this effect can be controlled by modal excitation. This possibility splits the interference mechanism into 2 types: general, where no dependence is established, and restricted where certain modes are excited.

Specifications	*Interference mechanism*		
	General	*Restricted*	
		Paired	*Symmetric*
Inputs x Outputs	N x N	2 x N	1 x N
First single image distance	$3L_\pi$	L_π	$3L_\pi/4$
First N-fold image distance	$3L_\pi/N$	L_π/N	$3L_\pi/4N$
Excitation requirements	none	$c_v = 0$ for $v = 2, 5, 8, ...$	$c_v = 0$ for $v = 1, 3, 5, ...$
Input(s) location(s)	any	$y = \pm W_e/6$	$y = 0$

Table 4.1: Summary of characteristics for the multiple interference mechanisms. [25]

Table 4.1 illustrates the interference types as well as their specifications (when necessary). In there, the W_e represents the effective width of corresponding fundamental mode, however, for waveguides with higher difference between n_r and n_c, this value is approximately W_M (ridge width Figure 4.2).

Also, there is a parameter c_v that represents the field excitation coefficients of each v mode [25].

4.1.1.1 General Interference

As it is possible to see by Table 4.1, general interference mechanism allows the construction of an MMI with M inputs and N outputs independent of the position and shape of the input fields as well as for excitation requirements.

In MMIs with general interference, the first single image will appear in multiple integer distances of $3L_\pi$ with multiple images interspersed at $\frac{3p}{2}L_\pi$ for $p = 1, 3, 5....$ However, experiments have shown that the performance of these devices can be further optimized by carefully positioning the access waveguides, leading to the Restricted Interference [25].

4.1.1.2 Restricted Interference

Restricted interference, as the name suggests, place restrictions on the modal excitation. In this mechanism, only some of the guided modes in the multimode waveguide are excited by the input. In restricted Interference, the MMI device can have two different mechanisms depending on the number of inputs : Paired (2 inputs) and Symmetric (1 input) Interference [25].

- Paired Interference

  Paired restricted interference, as the name suggests, requires 2 inputs. When compared to an MMI build with general interference for M = 2, the paired restricted interference MMIs achieves smaller dimensions once the first single image and the first N-fold image will appear at a shorter distance. Despite that, this mechanism, unlike the previous one, has excitation and input location requirements that must be obeyed (requirements described in Table 4.1) [25].

- Symmetric Interference

  Symmetric interference can only be used for MMI with one single input. This interference mechanism is the one who obtains the first single and N-fold images at shorter distances, and, consequently, small dimensions devices [25].

4.2 1x4 MMI Coupler design and results

As it was mentioned before, these devices became highly relevant for optical communications due to their properties and the several functions it may perform. The goal for this design is to accomplish a well balanced and low loss device for channel multiplexing of 4 channels in two bands : Downstream and Upstream.

The imbalance is defined as the maximum to minimum output power ratio for all M outputs, for an N x M MMI, expressed in dB. Accordingly to [25], these devices can provide insertion losses below 0.5 dB and balancing within 0.2 dB [25]. In order to obtain small loss values and well-balanced splitting, the multimode waveguide is required to support at least $N + 1$ modes.

Both MMIs are designed for SmartPhotonics foundry, using their stack. Foundry's design manual, provides two etched waveguides: shallow and deep. Soldano et al. indicates in [25] that deeply etched access waveguides provides increased fabrication tolerance for the device performance.

4.2.1 1x4 MMI Coupler design for C band

To start the design of the 1x4 MMI coupler, the stack provided by the foundry was designed and then implemented a structure with three sections: input access waveguides, multi mode waveguide and output access waveguides. Both access waveguides (input and output) were implemented with a straight waveguide connected to a taper waveguide. The addiction of tapered waveguides to connect the single mode guides with the multimode section, allows a more progressive transition from single mode to multimode propagation. This mechanism allows an optimization of the output power by control of the launched modes. The geometric structure implemented is illustrated by Figure 4.3.

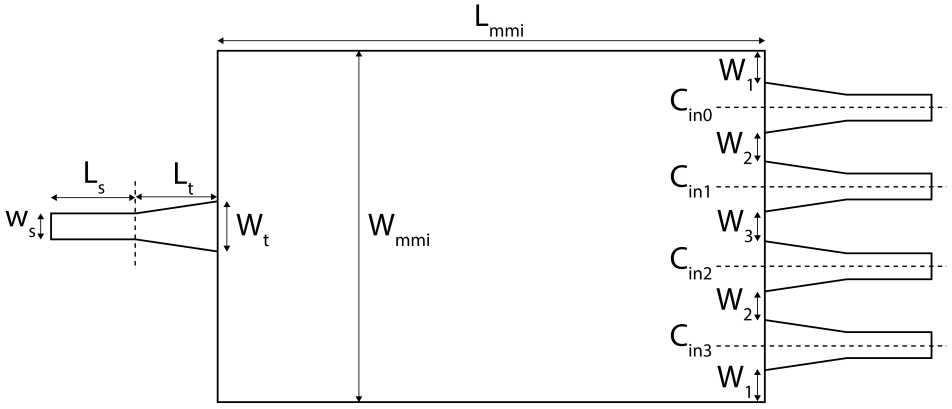

Figure 4.3: Geometric figure and parameters that make MMI's final structure.

The dimensions mentioned in Figure 4.3 are listed in Table 4.2.

Parameter	***Specification***			***Value*** (μm)
L_{mmi}	***Multimode section***		*length*	159
W_{mmi}			*width*	17
c_{in0}	***Access waveguides***	***Output waveguides center position***	*output 1*	6.5
c_{in1}			*output 2*	2.5
c_{in2}			*output 3*	-2.5
c_{in3}			*output 4*	-6.5
L_s		***Geometry***	*straight length*	50
L_t			*taper length*	50
W_d			*deep waveguides width*	2
W_t			*tapered facet width*	3
W_1	***Access waveguides margins***		*waveguide - border*	0.5
W_2			*waveguide-waveguide*	1.5
W_3				1

Table 4.2: Values discrimination of MMI's geometry dimensions represented in Figure 4.3. c_{in0}, c_{in1}, c_{in2} and c_{in3} are absolute values for y-axis, where y = 0 corresponds to the middle of the structure's width.

SmartPhotonics's design manual states for minimum space between deep waveguides the value of 0.8 μm, which was set as the minimum distance between waveguides in the structure.

To achieve the correct position of the output ports, a structure was simulated with 1000 μm length for multimode section with the access waveguides referred before in positions equally distributed along the MMI width. The result of an bidirectional Eigenmode Expansion (EME) propagation through this structure is shown in Figure 4.4.

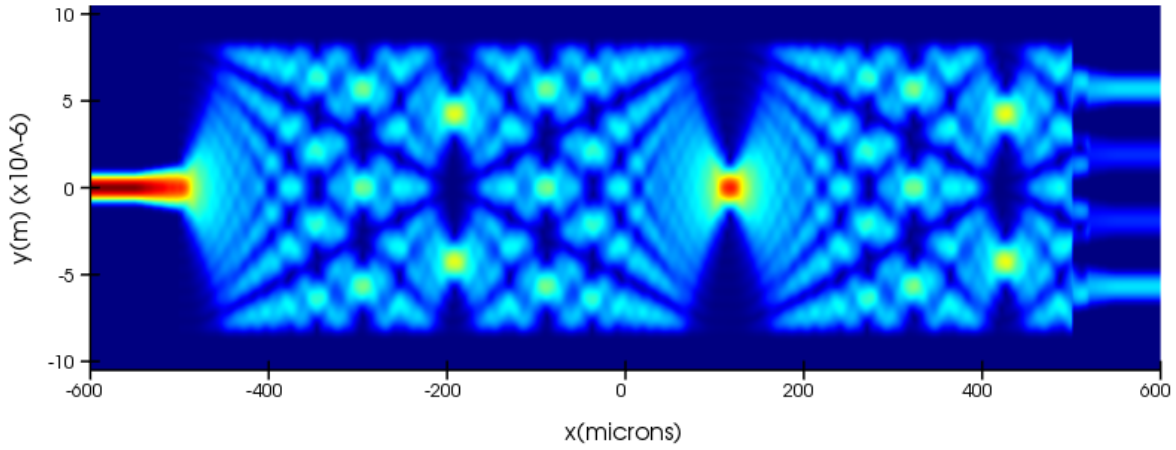

Figure 4.4: Field propagation over the XY plane of the structure for $\lambda = 1532.68nm$.

As it is possible to see in Figure 4.4, MODE software from Lumerical runs the EME propagation propagating light in through the x-axis, being y-axis the width of the structure, and the height of the structure in z-axis. Also, in Figure 4.4, it is possible to see a four image

field for, approximately, $x = -340\mu m$, for y-axis positions of c_{in0}, c_{in1}, c_{in2} and c_{in3} (Table 4.2). After positioning the output ports in these values, it was performed a propagation sweep through the MMI body length to find the S parameters between the input and the output ports closest to the ideal (once there are 4 output ports, the ideal normalized s_{1x} value for $x = 1, 2, 3, 4$ would be $1/4 = 0, 25$). The wavelength used to perform these tests was the first channel frequency of C band - 195.6 THz, corresponding to 1632.68 nm.

It was evaluated the transmission factor between ports for the lowest order mode for both TE and TM polarization. This is important because both polarizations have different characteristics: TM modes are more sensitive to the waveguide's height (z-axis) due to the confinement of the major component of the electric field in the vertical direction, while TE modes are not so sensitive to the height, but to the width of the waveguide (y-axis), mainly because its major component of the electric field [26]. Once the stack is composed by the foundry (heights values included) it is necessary to evaluate if, for a certain width, the structure presents a polarization dependency performance or not. Figure 4.5 presents the first lower mode, for TE and TM polarizations, transmission function for multiple MMI lengths.

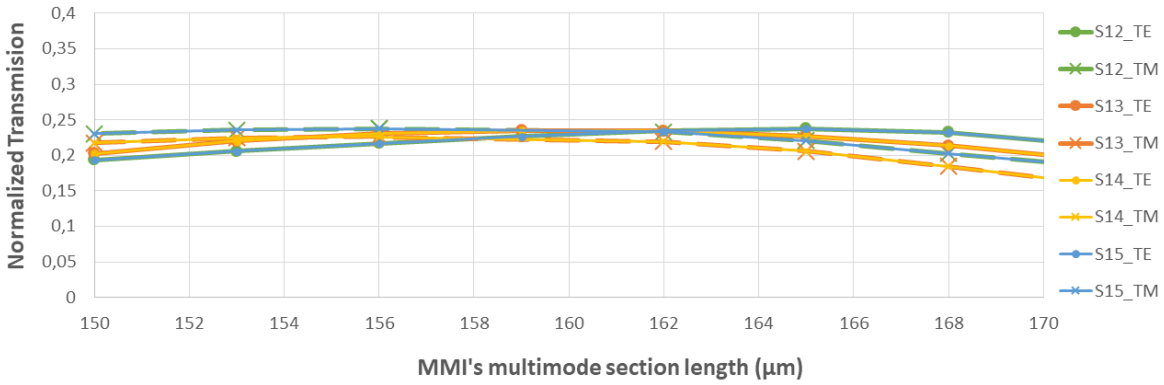

Figure 4.5: MMI transmission as a function of multimode section length for TE and TM modes ($\lambda = 1532.68$ nm).

For easier reading and interpretation of the results, each port is illustrated with a different color and for each one, the TM modes are represented by '×' points and dashed lines, while TE mode presents a '•' mark with continuous lines. The S1x parameters referred in Figure 4.5 represents the transmission normalized value from the input port (Port 1) to the four different output ports: S12 is referring to the transmission factor from the input to the output centered in c_{in0} from Figure 4.3, the same way as the S13, S14 and S15 represents for, respectively, the c_{in1}, c_{in2} and c_{in3} output centered from the same figure.

As it is possible to see in Figure 4.5, for the same output port, both polarizations presents slight different values. Despite that, for $L_{mmi} = 159\mu m$ the transmission values of every ports in both polarizations, present values very close to 0.25. Also, when comparing this to the point with similar transmission values ($L_{mmi} = 162\mu m$), the imbalance between ports is lower, providing better balance between ports at the output of the device. For these reasons this point was the length chosen for the MMI.

In Table 4.3 it is possible to evaluate the S parameters for all the 4 output ports as well as their corresponding insertion loss (in dB).

Modes	S_{12}		S_{13}		S_{14}		S_{15}		***Maximum Insertion loss***	***Maximum Imbalance***
		dB		**dB**		**dB**		**dB**		
TE	0.23	**-6.45**	0.24	**-6.24**	0.24	**-6.24**	0.23	**-6.45**	**0.44 dB**	**0.22 dB**
TM	0.24	**-6.24**	0.23	**-6.47**	0.23	**-6.47**	0.24	**-6.24**		

Table 4.3: S parameters for a MMI structure with geometry corresponding to values in Table 4.2.

The maximum insertion loss from Table 4.3 is calculated by the difference between the insertion loss of the ideal S parameter $(0, 25)$ and the insertion loss of the S-parameter with more deviation from this value. The maximum imbalance is calculated using the two extreme values (the higher and the lower values) of the S parameters. Insertion losses is given by

$$10log_{10}(s_{1x}) \tag{4.1}$$

for $x = 1, 2, ...N$, being N the number of output ports of the device.

With the complete structure defined, the final step was to evaluate the device performance along the wavelength band for NG-PON2, in this case, for 4 channels between 1532 nm and 1535 nm.

The performance of the device along the band is stated in Figure 4.6 for both TE and TM modes.

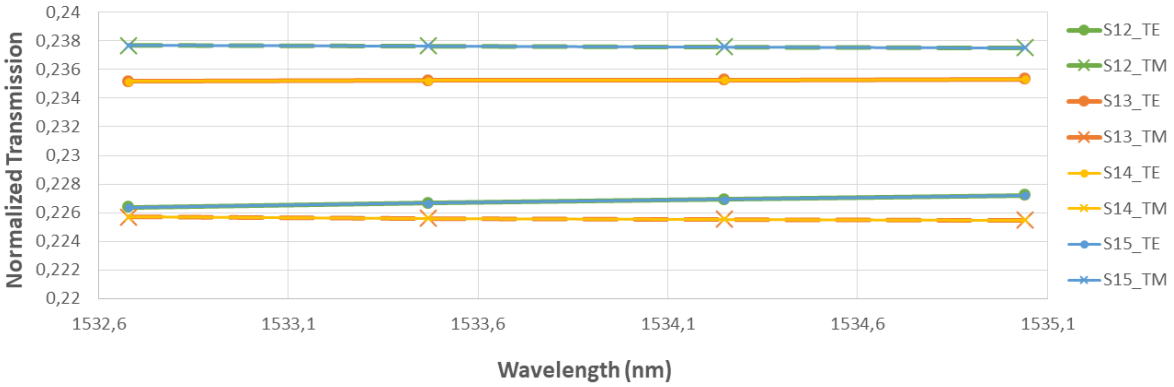

Figure 4.6: C band performance of the device.

As it is possible to see, the S parameters for every ports do not suffer significant variation along the band, being the maximum variation in the order of 10^{-3} what corresponds, in dB, to less than -30 dB variation between channels in the same band. Also, it is possible to see that output ports centered at the same distance from y axis presents similar values (S12 = S15 and S13 = S14) resulting in overlap of these values.

Having optimized the full structure MMI' design, it is also important to evaluate the device's tolerance to fabrication errors into device's performance. During actual device fabrication, the device's geometry may be affected by both lithography (the initial imaging of the device into the wafer) and etching processes, independently to any mask errors it may present previously. During lithography, many factors (as exposure dose, temperature humidity, etc) may introduce variations in the geometry face to the mask implementation, as well as during etching phase, for different dependency-factors (the etch time, degree of undercut, etc) [27].

In [28] fabrication margins of ±200 and ±100 nm were considered for MMI performance, for InP-based device. Once the foundry does not specify the safety margin for fabrication, this margins were considered and evaluated for this device's performance.

Figure 4.7, and 4.8 shows the insertion loss penalties as a function of MMI width.

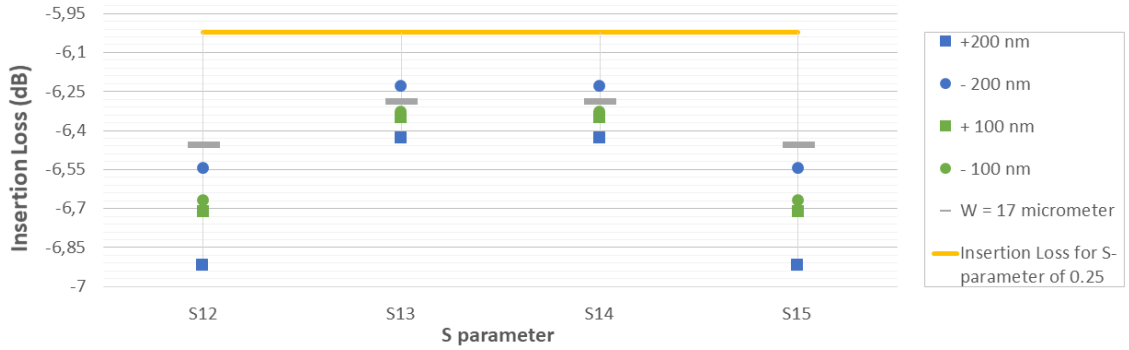

Figure 4.7: Insertion loss penalty due to MMI width variations of ± 100 and ± 200 nm for TE mode ($\lambda = 1532.68$ nm).

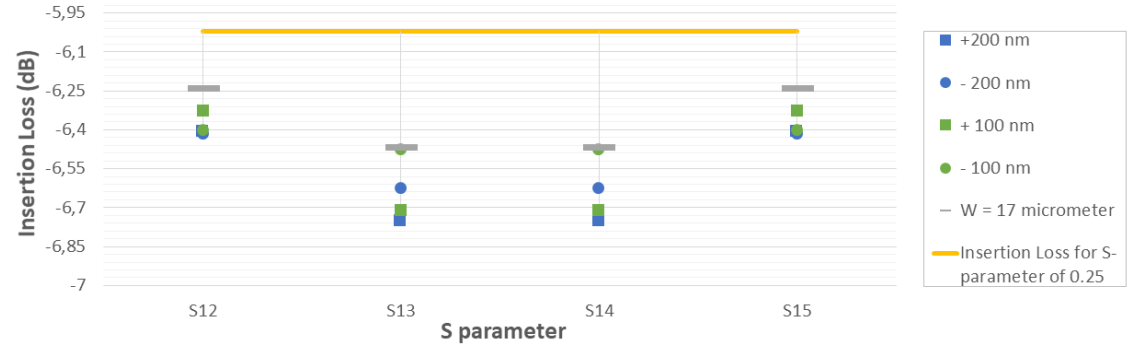

Figure 4.8: Insertion loss penalty due to MMI width variations of ± 100 and ± 200 nm for TM mode ($\lambda = 1532.68$ nm).

For easier interpretation of the results illustrated in graphs from Figures 4.7 and 4.8, the insertion loss from de design structure is stated by the grey trash while the nominal variations are represented by colors: blue for 200 nm variations and green for 100 nm variations. Also, for positive variations (more width) the values are represented with square marks while decrease width variations are represented with circle marks. It is also presented with a yellow continuous line the ideal value of insertion loss for a perfectly balanced MMI.

As it is possible to see in the previous figures, both TM and TE modes suffer differently with MMI's width variation.

For the output ports centered in c_{in1} and c_{in2} (Figure 4.3), represented in Figure 4.7 for the "S13" and "S14" S parameters, the variations do not represent a big impact in device performance, deviating less than 0.2 dB from the expected insertion loss. On the other hand, output ports represented in the same Figure by the "S12" and "S15" S parameters,

experiences a major impact of almost 0.5 dB in insertion loss, even if it does not represent a large difference, it becomes far from the desired value (approximately -6 dB).

Different from TE mode, TM mode presents major variations in insertion loss values from the inner ports (Figure 4.8 "S13" and "S14" parameters) rather than in border ports ("S12" and "S15" parameters from the same figure).

It is possible to conclude that, for these variations the polarization dependency of the structure becomes higher when comparing the performance from TE and TM polarizations.

Considering the total insertion loss introduced by the device of -6.36 dBm, the fabrication errors considered, will oscillate this value between -6.62 and -6.45 dBm.

The final propagation for TM and TE modes is illustrated in Figure 4.9a and 4.9b, respectively.

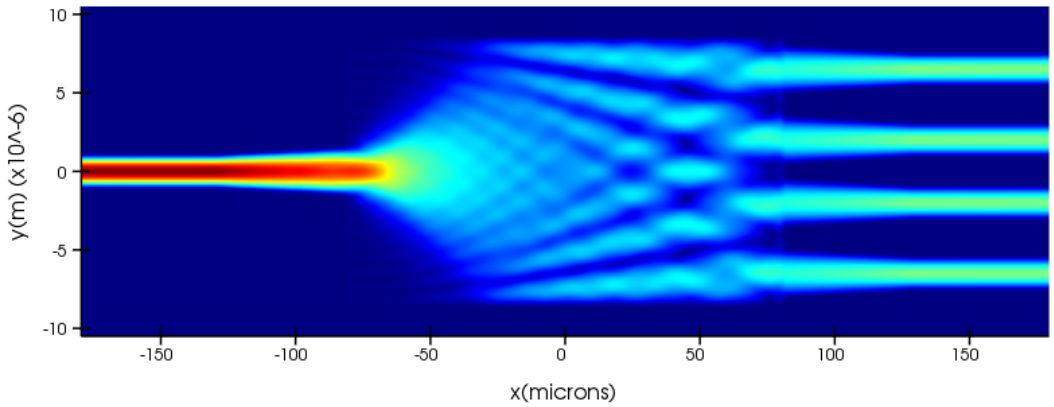

(a) TM mode propagation.

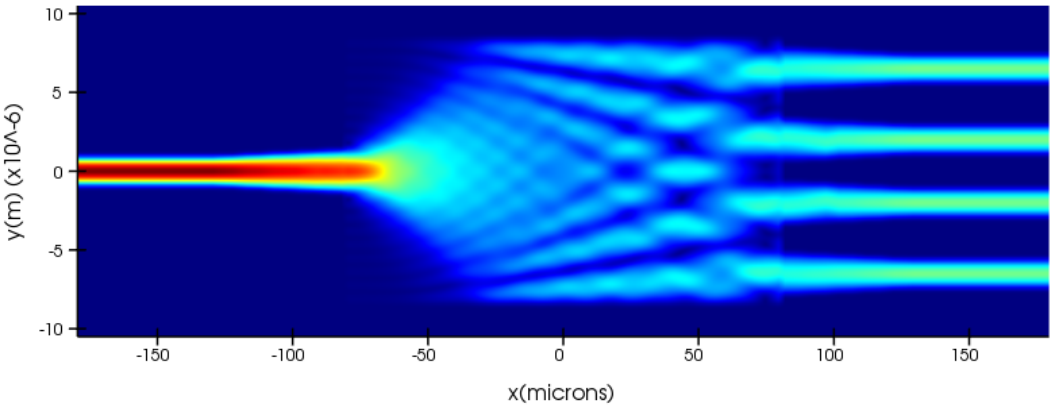

(b) TE mode propagation.

Figure 4.9: Full light propagation for a structure with parameters described in Table 4.2 for TE and TM modes ($\lambda = 1532.68$ nm).

4.2.2 1x4 MMI Coupler design for L band

Once the stack of materials and general structure is fixed (Figure 4.3), it is expected that the ideal geometric dimensions for the L band device results in similar values to the C band design. However, it is not expected to be the same due to the dependence of the refractive index to the wavelength. Once this device is projected to a different frequency band, it is expected to have deviation from the previous structure.

Repeating the first step of the designing process described before, it was possible to obtain an image of light propagation through the structure described in Figure 4.10.

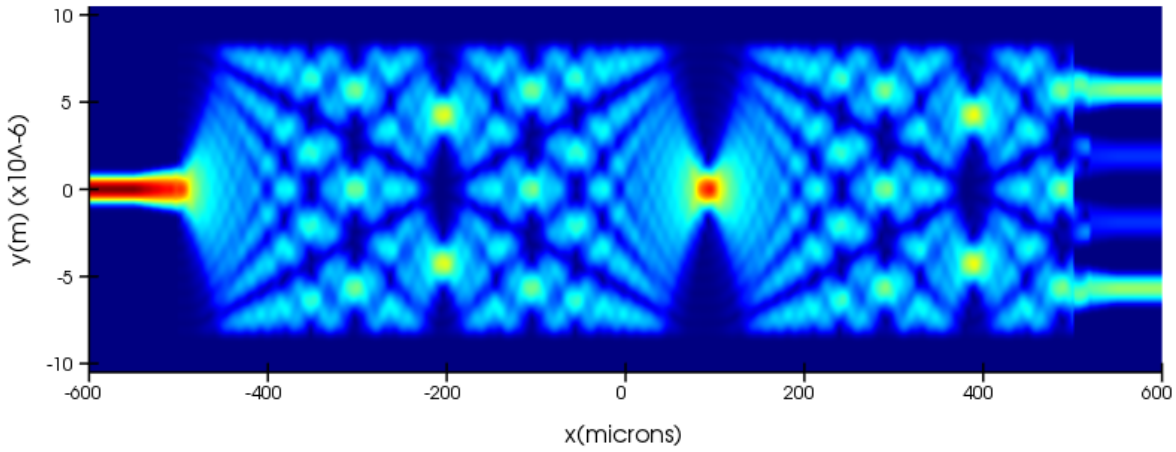

Figure 4.10: Field propagation over the XY plane of the structure for $\lambda = 1596.34nm$.

The 4-image formation is at approximately, $x = -350\mu m$. Once again, through this point, the center positions of the four output waveguides were obtained.

The next designing step is to determine the length of the multimode section of the MMI. The result of the EME propagation sweep for this parameter is placed in Figure 4.11.

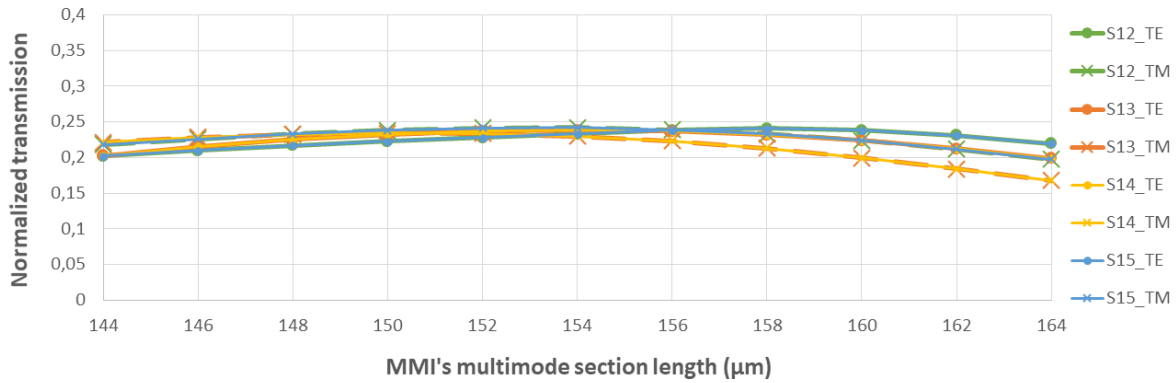

Figure 4.11: MMI transmission as a function of multimode section length for TE and TM modes ($\lambda = 1596.34nm$).

For the reasons stated previously, the point chosen to perform the length of the MMI is 154 μm. The performance of this device is described in Table 4.4.

Modes	S_{12}		S_{13}		S_{14}		S_{15}		***Maximum Insertion loss***	***Maximum Imbalance***
		dB		**dB**		**dB**		**dB**		
TE	0.23	**-6.32**	0.24	**-6.23**	0.24	**-6.23**	0.23	**-6.33**	**0.3626 dB**	**0.2189 dB**
TM	0.24	**-6.23**	0.23	**-6.33**	0.23	**-6.33**	0.24	**-6.23**		

Table 4.4: S parameters for a MMI structure with geometry corresponding to values scripted in Table 4.5.

The final geometric measures for the obtained MMI, corresponding to Figure 4.3, are listed in Table 4.5.

Parameter	***Specification***			***Value*** (μm)
L_{mmi}	***Multimode section***		*length*	154
W_{mmi}			*width*	17
c_{in0}	***Access waveguides***	***Output waveguides center position***	*output 1*	6.5
c_{in1}			*output 2*	2.5
c_{in2}			*output 3*	-2.5
c_{in3}			*output 4*	-6.5
L_s		***Geometry***	*straight length*	50
L_t			*taper length*	50
W_d			*deep waveguides width*	2
W_t			*tapered facet width*	3
W_1	***Access waveguides margins***		*waveguide - border*	0.5
W_2			*waveguide-waveguide*	1.5
W_3				1

Table 4.5: MMI's geometry dimensions (L band).

It was also evaluated the performance along the DS NG-PON2 band. The results are presented in Figure 4.12.

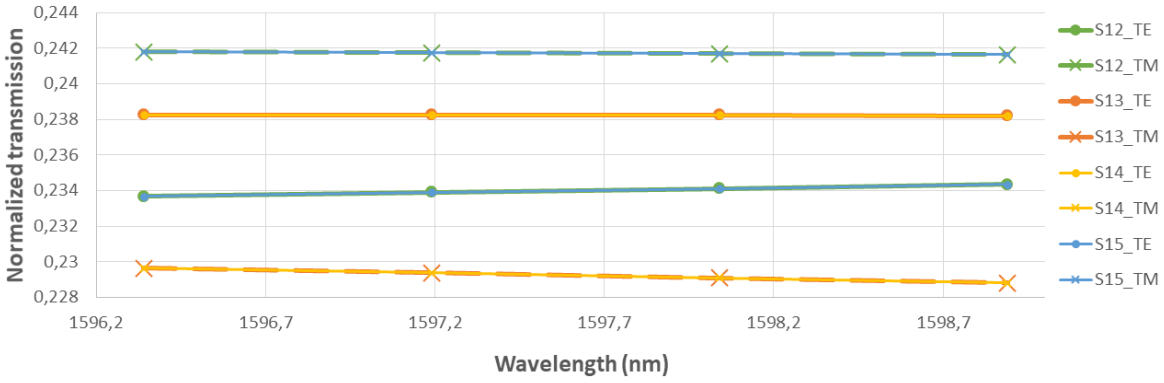

Figure 4.12: L band performance of the MMI.

It is possible to see that variations along the band were similar to the observed in the previous structure, which is still a negligible value for variation along the band.

The full propagation in the structure of multimode interference where the interferometric pattern and light propagation can be evaluated in Figure 4.13a and 4.13b for TM and TE modes, respectively.

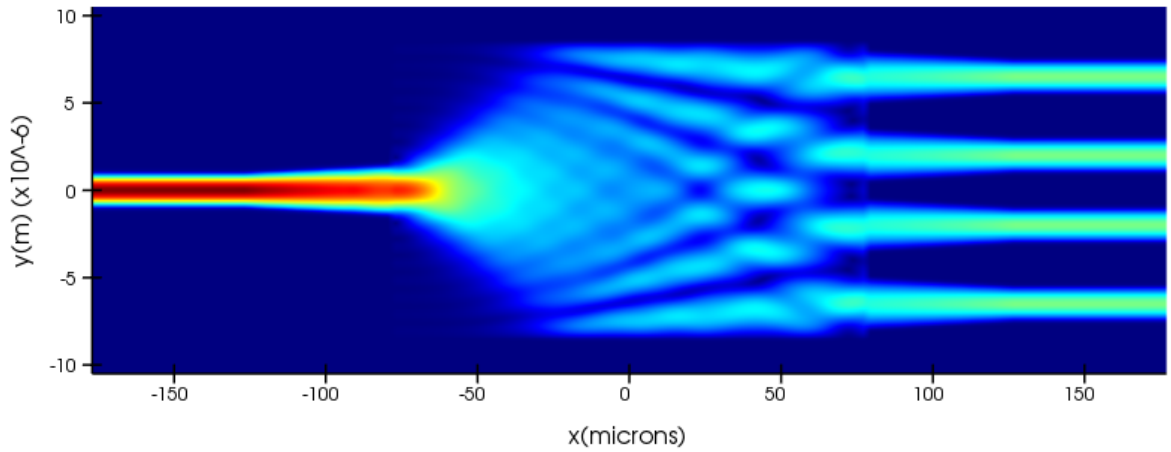

(a) TM mode propagation.

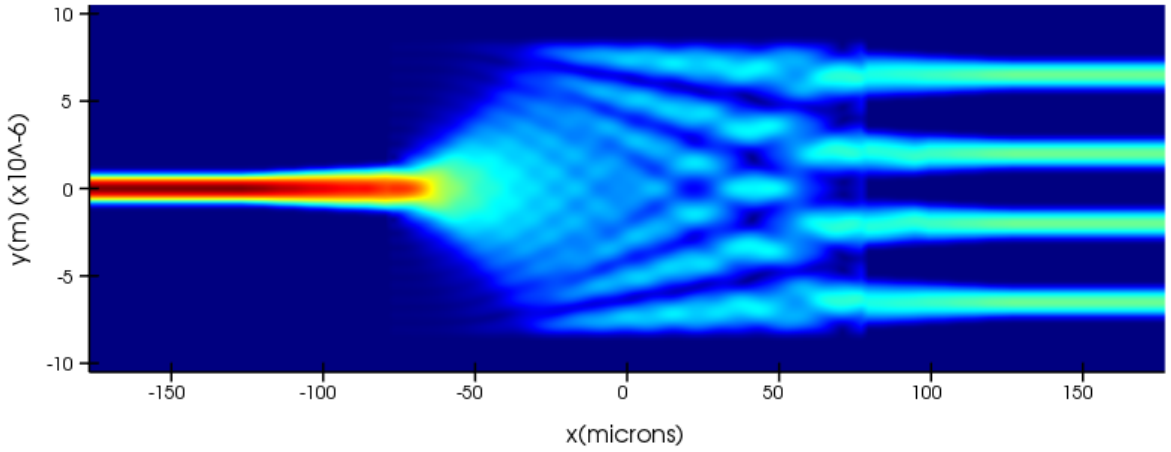

(b) TE mode propagation.

Figure 4.13: Full light propagation for a structure with parameters described in Table 4.5 for TE and TM modes($\lambda = 1596.34nm$).

To conclude the designing process, the last step was to analyse the structure resilience to the multimode section width of $\pm$ 200 and $\pm$ 100 nm (similarly to the process in the previous section).

Figure 4.14 and 4.15 show the insertion loss variations for the fabrication error considered

for TE and TM modes.

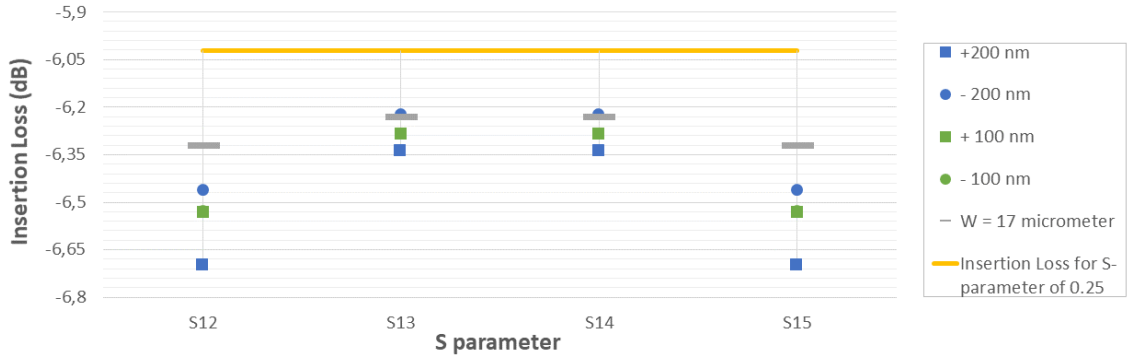

Figure 4.14: Insertion loss penalty due to possible fabrication errors of ± 100 and ± 200 nm in multimode section width, for TE mode propagation ($\lambda = 1596.34nm$).

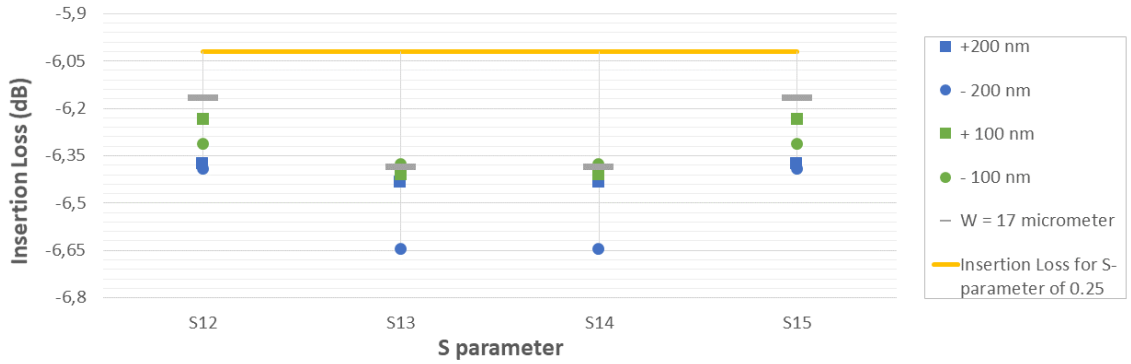

Figure 4.15: Insertion loss penalty due to possible fabrication errors of ± 100 and ± 200 nm in multimode section width, for TM mode propagation ($\lambda = 1596.34nm$).

Analyzing Figures 4.14 and 4.15 it is possible to see that for both propagation modes, the fabrication errors considered, will suffer an impact from the insertion loss of the device up to a maximum of approximately 0.4 dB.

Considering that the overall insertion loss of the designed device is -6.27 dBm, for the two worst scenarios of fabrication error estimated (± 200 nm) the insertion loss will vary between -6.46 and -6.43 dBm.

Chapter 5

ONT transmitter architecture for NG-PON2 systems

Concluding all studied until this moment, it is now time to apply to the design of an ONT for NG-PON2 systems. The aim of this chapter is to report the procedure to implement a proposal architecture of a PIC to perform a ONT transmitter with channel bonding, allowing this chip to achieve a bit rate up to 40 Gbit/s (using the minimum channel number established by standard NG-PON2). The proposed architecture should be a generical one, so it is possible to reproduce it for several foundries. In this case it was design with FhG-HHI foundry design rules using OptoDesigner software.

This chapter is divided into 2 main parts: the first one presents the blocks used to compose the architecture as well as the final block diagram of the transceiver. Later, the final mask layout is presented concerning the foundry Process Design Kit (PDK) made available by FhG-HHI foundry.

5.1 Transceiver Architecture

In chapter 2 of this work, it is mentioned that NG-PON2 systems are typically implemented with an ONT with tunable lasers. Also, in the same chapter it is mentioned that it is possible to achieve more than 10 Gbit/s bit rate. To do that, channel multiplexing is explored to ensure a bandwidth flexible management increasing the number of channels received by each ONU/ONT up to 4x10 Gbit/s. Also, every PON systems provides two bands: DS for transmission data from OLT to ONU/ONT and US for the opposite direction transmission data. The DS transmission must be implemented in OLT transceivers with the respective reception located in the ONT, being the US band implemented inversely. This architecture is planned to implement a transmitter ONT, so it must present transmission located in the US range, with a minimum output power of 8 dBm. As seen in simulation results from chapter 3, external modulation presents higher Q-factor values relatively to direct modulation and, therefore, it was the simulation type chosen to implement in this architecture. Lastly, all must be according with the requirements specified in Table 2.5. To do that, the block diagram represented in Figure 5.1 was proposed.

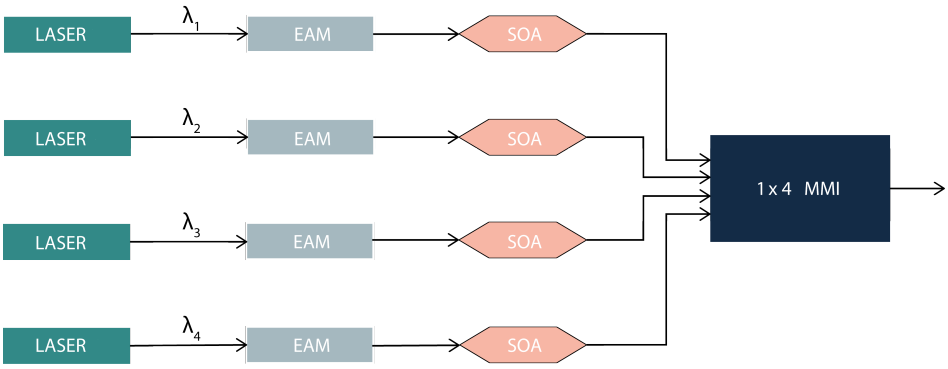

Figure 5.1: Diagram block for the proposed architecture for OLT and ONT transmitter.

There are four DFB lasers transmitting each one at one specific channel (wavelengths specified in Table 5.1), then external modulation takes place through EAM blocks and then light is amplified. Channel multiplexing is performed by a MMI that combines outputs to the fiber to be propagated through ODN to OLT's transceivers.

Parameter	*Wavelength (nm)*
λ_1	1532.68
λ_2	1533.46
λ_3	1534.26
λ_4	1535.04

Table 5.1: Operating wavelength for each laser illustrated in Figure 5.1.

5.1.1 Building Blocks

The MMI used to implement the architecture described in Figure 5.1 was the one implemented in the previous chapter, for the C band. The characteristics of that block can be found in the section 4.2.1 of this document. Despite that, building blocks were also used to implement this architecture. In the following sub sections, the characteristics of the chosen BB will be presented.

5.1.1.1 Distributed Feedback Laser

For this architecture it was necessary to ensure that channels frequencies were correctly defined. As mentioned previously in chapter 3, DFB lasers allows the calibration of its light generation to a specific wavelength value through the current injection and its temperature dependency.

These blocks have two optical ports where light is transmitted, and five electrical ports : 3 for the Ground-Signal-Ground (GSG) structure and 2 for the electrical tuning of wavelength.

According to [29], for a 1530 nm wavelength output and a 9 dBm of output power (as stated in Table 2.5), it is necessary to apply to the DFB block, a 100 mA current.

5.1.1.2 Electro-Absorption Modulator

As seen in chapter 3, EAM are modulators with working principle based on changing the RI of the material by means of electric current injection. Accordingly to [30], these blocks are very attractive to optical communications for high bandwidths, due to several characteristics: short length (very important for PIC), an order of magnitude lower than phase modulators, and their high ER.

Accordingly with the foundry, for a 100 μm length modulator, it is possible to achieve an ER of 10 dBm, for a voltage applied of 2 V. This block also introduces a 5 dB power loss to the system.

Besides the optical signal, the block also receives the electrical signal to be modulated by a GSG.

5.1.1.3 Semi-conductor Optical Amplifier

The SOA block main function is to add a signal boost to the system. However, it is necessary to take in concern the possibility to amplify noise at the same time the signal is amplified. Adding to that, the dimension constraints of the chip favors the smallest length choice for this device, although the smaller it gets, the less it is able to amplify.

Accordingly with the foundry, it is possible to achieve a 10.6 dB for gain, for a 900 μm length with 200 mA of injected current.

This block has two optical ports and two electrical ones for the electric pumping.

5.2 Final mask layout

In Figure 5.2 it is possible to see the final mask layout of the architecture without the DC tracks and pads.

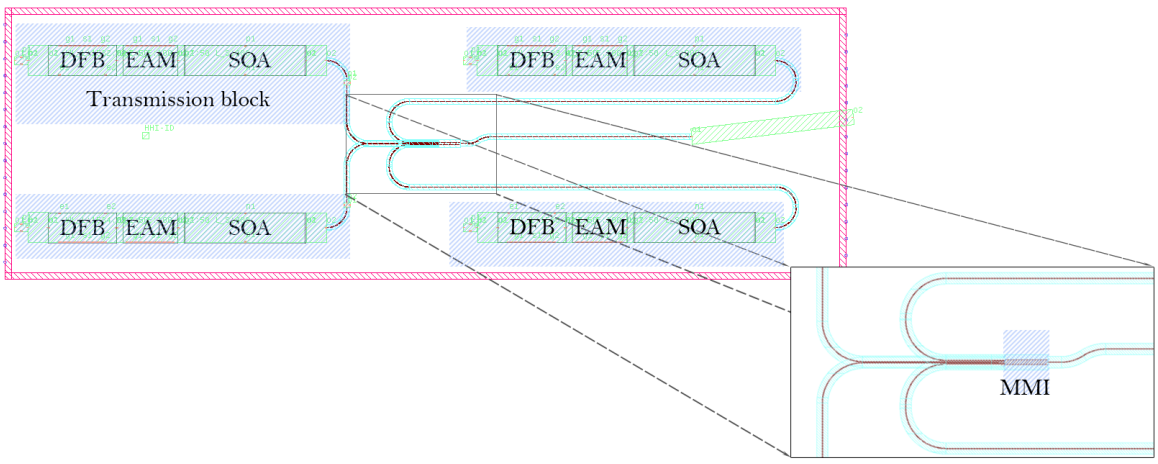

Figure 5.2: Final architecture mask layout.

In Figure 5.2 it is possible to see four transmission blocks for the four channels to be transmitted (two in the upper side and other two in the bottom side).

The final power budget is described in Table 5.2.

Parameter	***Value***
DFB Laser	+9 dBm
EAM modulator	-5 dB
SOA	+10.6 dB
MMI	-6.36065 dB
Total output transceiver power	+8.23935 dBm

Table 5.2: Optical power budget in transceiver architecture.

In the construction of this architecture, it was verified the necessity to add a few more blocks to the structure than it was mentioned in Figure 5.1.

Firstly, the DFB blocks from FhG-HHI are composed by two optical ports. In order to avoid reflections inside the chip, originated by the output light from the unused optical port of this block, it was connected to a photodetector. This block absorbs the light from one of the output ports of the laser, and, it was then connected to DC pads in order to enable an additional verification, called power monitoring.

The foundry provides active blocks with and without joints to couple active to passive blocks. One can conclude that, once it was necessary to connect several active blocks right after each other, in order to save space in the chip, it was preferable to use active blocks without joints and add only two butt-joint blocks in the extremities (one between the debug photodiode and the laser and another one in the SOA). Between the DFB, the EAM and the SOA, isolator blocks to isolate p-regions between them were used.

In order to reduce the wire bonding costs when introducing this chip into the printed circuit board, the DC pad connections must be implemented as close as possible to the chip's borders. Besides that, it also must be considered the minimum spacing between them of 150 μm, being its form a rounded square with (100 x 100) μm^2.

These factors were determinant in the final disposition of the building blocks in the chip always taking in concern the smallest chip area usage.

With all that in mind, it was necessary to study if this composition adds thermal crosstalk effect due to the proximity of the DFB between themselves. Accordingly to [31], a safety margin for thermal interference between two DFB lasers is approximately 300 μm in x-axis and 420 μm in the y-axis. The architecture presented in Figure 5.2 presents minimum separations between lasers of 2800 μm in the x-axis and 1000 μm in the y-axis. One can conclude that there is no thermal crosstalk between the DFBs using this geometry.

Last, the final building block added to the architecture is a Spot-Size Converter (SSC). This block is used to connect the transceiver to the optical fiber. It is implemented with a 7 $^\circ$ rotation from x-axis to reduce internal reflections in the chip. This building block is characteristic from the foundry and it may not be necessary when implementing this architecture into, for example, SmartPhotonics foundry.

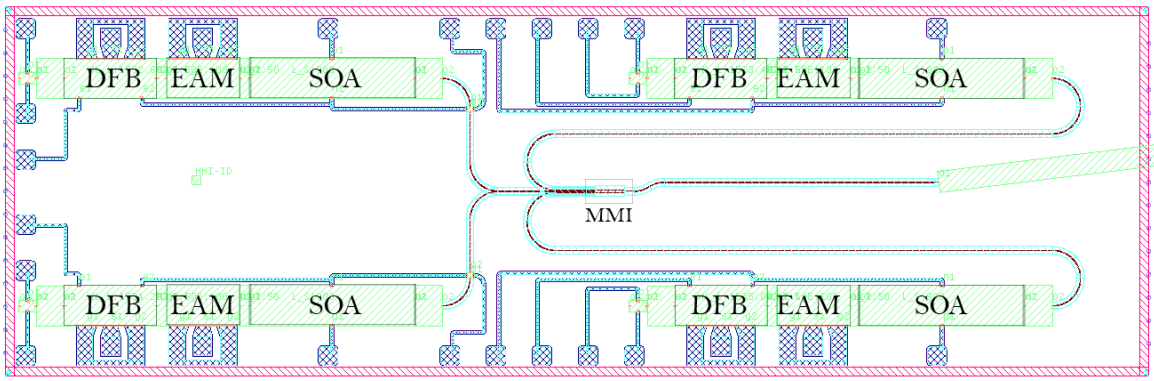

Figure 5.3: Mask layout of the ONT transmitter.

To conclude the chip design, the Optodesigner software provides a Design Rule Check that evaluates if all the foundry design requirements (minimum radius, connections, spaces, etc) are respected. Concluding this test successfully, the final mask layout from Figure 5.3 is obtained.

Chapter 6

Conclusions and Future Work

6.1 Conclusions

The main focus of this thesis was to propose a PIC architecture for an ONT transmitter for the minimum required by NG-PON2 of 4 channels with an aggregate bit rate of 40 Gb/s made available by the use of channel multiplexing. It was also necessary to guaranty an 8 dBm output power minimum.

Right after a brief introduction of the optical communications theme, where the final users demand for higher bit rates and bandwidth, and, consecutively, the telecommunications's operators also increasing demand, was presented as the main purpose for optical communications and PONs development and fabrication, a brief introduction to the document's structure was presented.

Then, the study starts with a PON's characteristics survey as well as the currently standard in development, the NG-PON2. Concluding the technical aspects of the network implementation, it was then introduced the integrated optics (PICs) technology stating facts as nowadays industry, the materials used, and foundries such as SmartPhotonics and FhG-HHI, both mentioned in the later work. It was concluded that InP based PICs were the ideal option to implement the architecture, ensuring a final architecture with speed enhancement at the same time it is reduced the power consumption as low as possible and yet increasing reliability.

In order to get familiarized with optical components, some of them necessary to implement later in the architecture design, each was described. For that, lasers, Optical fiber(representing the passive waveguides in PIC), SOA and photodetectors were discussed. Right after, the working flow of these components were simulated in a complete transmission-reception system using Lumerical's software INTERCONNECT to evaluate direct versus external modulation performance. As it was mentioned in the optical components's discussion firstly, the results showed that external modulation presents better results (higher signal quality factor) than direct modulation, and, for that reason, external modulation was chosen as the modulation to be implemented in the purposed architecture.

To implement channel multiplexing, the self-imaging principle was then studied in order to design and implement an 1x4 MMI for both transmission and reception NG-PON2 bands for SmartPhotonics foundry. This dissertation provides a full step design to implement this block using MODE software from Lumerical resulting in two well balanced and low loss couplers.

Concluding the major goal of this dissertation, the final step was the proposal of an archi-

tecture for the ONT. It was firstly presented an overall overview of the proposal architecture by the use of a block diagram and then presented the BB that integrates this proposal from FhG-HHI. This dissertation finishes with a complete mask layout of the chip, ready to be produced.

6.2 Future Work

Although the major goal for this thesis was concluded, there are several iterations that, investing more time, could be interesting to achieve:

- The MMI implemented in the proposal architecture was designed and tested for Smart-Photonics foundry. One possible optimization was the performance evaluation in FhG-HHI foundry stack, to guarantee the loss and imbalance result values.
- A further study of the BB SOA behaviour and performance could improve its design, possibly with a size reduction of this component reducing the overall chip size.
- Adding a receiver block in the architecture presents to be an enriching iteration to this work for increasing the useage of this architecture.
- The proposal architecture performance could be tested and analysed in a software simulation to prove the concept.

Bibliography

[1] Curtis Knittle. IEEE 100 Gb/s EPON. In *Optical Fiber Communication Conference*, pages Th1I–6. Optical Society of America, 2016.

[2] Gerd Keiser. FTTx concepts and applications. 2006.

[3] Dora. Evolution of the GPON technology. 2018. https://support.huawei.com/huaweiconnect/carrier/en/thread-445959.html. Accessed: 2019-10-21.

[4] Paulo P Monteiro, Diogo Viana, João da Silva, Diogo Riscado, Miguel Drummond, Arnaldo SR Oliveira, Nelson Silva, and Paulo Jesus. Mobile fronthaul RoF transceivers for C-RAN applications. In *2015 17th International conference on transparent optical networks (ICTON)*, pages 1–4. IEEE, 2015.

[5] VPIphotonics. Introduction to optical transmitters tx1 - lecture series. Technical report, Univeristy Program, Photonics Curriculum Version 8.0.

[6] John M Senior and M Yousif Jamro. *Optical fiber communications: principles and practice*. Pearson Education, 2009.

[7] Josep Prat et al. Next-generation ftth passive optical networks. *Springer Science+ Business Media B.*, 5, 2008.

[8] Ph Chanclou, F Bourgart, B Landousies, S Gosselin, B Charbonnier, N Genay, A Pizzinat, F Saliou, B Le Guyader, B Capelle, et al. Technical options for ngpon2 beyond 10g pon. In *European Conference and Exposition on Optical Communications*, pages We–9. Optical Society of America, 2011.

[9] Cedric F Lam. *Passive optical networks: principles and practice*. Elsevier, 2011.

[10] Nima Afraz, Amr Elrasad, Hamed Ahmadi, and Marco Ruffini. Inter-operator dynamic capacity sharing for multi-tenant virtualized PON. In *2017 IEEE 28th Annual International Symposium on Personal, Indoor, and Mobile Radio Communications (PIMRC)*, pages 1–6. IEEE, 2017.

[11] Derek Nesset. NG-PON2 technology and standards. *Journal of Lightwave Technology*, 33(5):1136–1143, 2015.

[12] ITU-T. Recommendation G.989.2 : 40-Gigabit-capable Passive Optical Networks 2 (NG-PON2): Physical Media Dependent (PMD) layer specification. *ITU*, 2019.

[13] ITU-T. Recommendation G.652 : Characteristics of a single-mode optical fibre and cable. *ITU*, 2016.

[14] Meint Smit, Siang Oei, Fouad Karouta, Richard Notzel, Joachim Wolter, Erwin Bente, Xaveer Leijtens, Jos van der Tol, Martin Hill, Harm Dorren, et al. Photonic integrated circuits: where are the limits? In *Integrated Photonics Research and Applications*, page IWB1. Optical Society of America, 2005.

[15] D Liang and JE Bowers. Photonic integration: Si or InP substrates? *Electronics Letters*, 45(12):578–581, 2009.

[16] JEPPIX. JePPIX MPW platforms. http://www.jeppix.eu/performance-summary-table. Accessed: 2018-11-19.

[17] Harry JR Dutton. *Understanding optical communications*. Prentice Hall PTR New Jersey, 1998.

[18] William Shieh and Ivan Djordjevic. *OFDM for optical communications*. Academic Press, 2009.

[19] Hiroyuki Ishii, Yasuhiro Kondo, Fumiyoshi Kano, and Yuzo Yoshikuni. A tunable distributed amplification DFB laser diode (TDA-DFB-LD). *IEEE Photonics Technology Letters*, 10(1):30–32, 1998.

[20] Ning Cheng and Frank Effenberger. WDM PON: Systems and technologies. In *European Conference and Exhibition on Optical Communication*, 2010.

[21] Govind P Agrawal. *Fiber-optic communication systems*, volume 222. John Wiley & Sons, Inc, 2002.

[22] Christophe Peucheret. Direct and external modulation of light. *Technical University of Denmark, Denmark*, 2009.

[23] Michael J Connelly. *Semiconductor optical amplifiers*. Springer Science & Business Media, 2007.

[24] Hari Singh Nalwa. *Photodetectors and fiber optics*. Elsevier, 2012.

[25] Lucas B Soldano and Erik CM Pennings. Optical multi-mode interference devices based on self-imaging: principles and applications. *Journal of lightwave technology*, 13(4):615–627, 1995.

[26] Andrés Sosa Andrade. Design of a silicon photonic multimode interference coupler. 2012.

[27] Harry-Dean Kenchington Goldsmith, Nick Cvetojevic, Michael Ireland, and Stephen Madden. Fabrication tolerant chalcogenide mid-infrared multimode interference coupler design with applications for bracewell nulling interferometry. *Optics express*, 25(4):3038–3051, 2017.

[28] D Pustakhod, X Jiang, EM Van Vliet, KA Williams, and XJM Leijtens. Characterization of 3x3 and 4x4 multimode interference couplers in InP generic photonic integration

technology. In *20th Annual Symposium of the IEEE Photonics Benelux Chapter, November 26-27, 2015, Brussels, Belgium*, pages 35–38. OPERA-photonics, Brussels School of Engineering, 2015.

[29] Fraunhofer HHI. Photonic InP foundry designmanual. 2019.

[30] Marija Trajkovic, Helene Debregeas, Kevin A Williams, and Xaveer JM Leijtens. 20 gbps operation of the electro-absorption modulator in the COBRA generic integration platform. In *Proc. 18th Eur. Conf. Integr. Opt.(ECIO 2016)*, pages P–39, 2016.

[31] Filipe Almeida Costa. Packaging of photonic integrated circuits for PON networks. Master's thesis, Universidade de Aveiro, Portugal, 2018.